ELSEVIER

# Trace element partitioning between majoritic garnet and silicate melt at 10–17 GPa: Implications for deep mantle processes

Alexandre Corgne [a,b,c,*], Lora S. Armstrong [a,d], Shantanu Keshav [a,e], Yingwei Fei [a], William F. McDonough [f], William G. Minarik [g], Karen Moreno [c]

[a] Geophysical Laboratory, Carnegie Institution of Washington, 5251 Broad Branch Road, NW, Washington, DC 20015, USA
[b] Institut de Recherche en Astrophysique et Planétologie, Université de Toulouse – CNRS, 14 avenue Edouard Belin, 31400 Toulouse, France
[c] Instituto de Geociencias, Universidad Austral de Chile, Casilla 567, Valdivia, Chile
[d] School of Earth Sciences, University of Bristol, Bristol BS8 1RJ, United Kingdom
[e] Géosciences Montpellier, Université de Montpellier – CNRS, 60 place Eugène Bataillon, 34 095 Montpellier Cedex 05, France
[f] University of Maryland, Department of Geology, College Park, MD 20742, USA
[g] McGill University, Department of Earth and Planetary Sciences, 3450 University Street, Montreal, Canada H3A 2A7

## ARTICLE INFO

## ABSTRACT

Melting experiments were performed on a silica-rich peridotite composition at 10–17 GPa to determine majoritic garnet–melt partition coefficients (D) for major and trace elements. Our results show that D for many elements, including Na, Sc, Y and rare earth elements (REE), varies significantly with increasing pressure or proportion of majorite component. Lu and Sc become incompatible at 17 GPa, with D decreasing from 1.5 at 10 GPa to 0.9 at 17 GPa. As predicted from lattice strain, log D for isovalent cations entering the large site of majoritic garnet exhibits a near-parabolic dependence on ionic radius. Our data are used to refine a previously published predictive model for garnet–melt partitioning of trivalent cations, which suffered from a lack of calibration in the 10–20 GPa range. Our results suggest that Archean Al-depleted komatiites from Barberton (South Africa) may have been generated by partial melting of dry peridotite at depths between 200 and 400 km. We also speculate that transition zone diamonds from Kankan (Guinea), which contain inclusions of majoritic garnet, may have formed from the partial reduction of $CO_2$-rich magmas that subsequently transported them to the surface. This hypothesis would provide an explanation for the REE patterns of majoritic garnet trapped within these diamonds, including Eu anomalies. Finally, we show that segregation of majoritic garnet-bearing cumulates during crystallisation of a deep Martian magma ocean could lead to a variety of Lu/Hf and Sm/Nd ratios depending on pressure, leading to a range of $\varepsilon^{143}Nd$ and $\varepsilon^{176}Hf$ isotope signatures for potential mantle sources of Martian rocks.

## 1. Introduction

Majoritic garnet is with olivine and its high-pressure polymorphs one of the main constituents of the deep upper mantle and transition zone of both Earth and Mars (e.g. Bertka and Fei, 1997; Ringwood, 1991). To understand the distribution of trace elements in the mantle of these planets, it is therefore crucial to constrain how trace elements dissolve in these minerals. Since fractionation of elements between different planetary reservoirs almost invariably takes place through processes of melting and crystallisation, it is appropriate to consider element distributions in terms of partitioning between minerals and melts. Majoritic garnet is of particular importance because it is the first mineral to crystallise from a peridotitic silicate melt (i.e. the liquidus phase) at pressures greater than ~14 GPa (e.g., Zhang and Herzberg, 1994). However, to date, limited partitioning data are available to model the geochemical consequences of crystallisation or melting in the stability field of majoritic garnet. Most of published garnet–melt partition coefficients of trace elements have thus far been obtained at pressures less than ~3 GPa (e.g., Fujinawa and Green, 1997; Hauri et al., 1994; Johnson, 1998; Nicholls and Harris, 1980; Salters and Longhi, 1999; Shimizu and Kushiro, 1975; van Westrenen et al., 1999, 2000a). Owing largely to technical issues, there are only a small number of data at higher pressures. Since garnet is progressively more enriched in the majorite component ($MgSiO_3$) at higher pressures and temperatures (e.g., Irifune, 1987), trace element partitioning patterns in the deep asthenosphere and transition zone are likely to be different from those at lithospheric levels. Therefore, low-pressure garnet–melt partitioning data are potentially unsuitable to model mantle melting or crystallisation at greater depths. Kato et al. (1988) and Ohtani and co-workers (Ohtani et al., 1989; Yurimoto and Ohtani, 1992) reported

* Corresponding author at: Instituto de Geociencias, Universidad Austral de Chile, Casilla 567, Valdivia, Chile. Tel./fax: + 56 63 22 12 08.
E-mail addresses: acorgne@irap.omp.eu (A. Corgne), l.armstrong@bristol.ac.uk (L.S. Armstrong), keshav@gm.univ-montp2.fr (S. Keshav), fei@gl.ciw.edu (Y. Fei), mcdonoug@umd.edu (W.F. McDonough), minarik@eps.mcgill.ca (W.G. Minarik), dinohuella@yahoo.com (K. Moreno).

pioneering results for a small number of lithophile trace elements over the 15–24 GPa and 16–20 GPa pressure ranges, respectively. These studies revealed that partition coefficients for heavy rare earth elements (REE) decrease substantially with increasing pressure while those for light REE may increase slightly. However, run durations were extremely short in these early experiments and chemical equilibrium may not have been completely attained, casting doubts on the accuracy of these first results. More recently, Draper et al. (2003) and Dwarzski et al. (2006) presented new data between 3 and 9 GPa, underlining the effect of pressure on garnet–melt partitioning of trace elements, respectively using Martian- and lunar-type compositions. Finally, Walter et al. (2004) and Corgne and Wood (2004) provided partition coefficients for a large number of trace elements at about 23 and 25 GPa, respectively, i.e. approximately at the deepest levels of the garnet stability field in the mantles of Earth and Mars.

The aim of this experimental study was to generate high-quality majoritic garnet–melt partition coefficients for a series of lithophile trace elements at pressures of the deep asthenosphere and transition zone. Experiments were carried out using a silica-rich peridotite starting composition at 10, 15 and 17 GPa to cover a wide range of pressure and generate data complementary to the existing data set. A first objective was to use our new data together with literature data to constrain further the systematics of trace element partitioning as a function of pressure. These new data have also been used to test current predictive partitioning models (Draper and van Westrenen, 2007; van Westrenen and Draper, 2007) and geobarometers based on majoritic garnet composition (e.g., Collerson et al., 2010). A second objective was to use our partition coefficients to model deep mantle processes in the stability field of majoritic garnet and shed light on the origin of Al-depleted komatiites, the formation of diamonds containing inclusions of majoritic garnets, and the chemical differentiation of a putative Martian magma ocean.

## 2. Experimental and analytical techniques

The starting material used in this study is a silica-rich peridotite composition. The major element composition determined by X-ray fluorescence (XRF) on a split portion of the starting material is given in Table 1. It is characterised by a molar Mg/Si ratio of ~1.1 as in carbonaceous chondrites, and by a molar Mg/[Mg + Fe] ratio (hereafter Mg#) of ~0.88. The reasons for choosing this composition rather than a fertile peridotite composition were two-fold: (1) cosmochemical comparisons suggest that terrestrial planets like Earth and Mars are potentially made of carbonaceous chondrites (e.g. McDonough and Sun, 1995); (2) a relatively low Mg/Si ratio should enhance the crystallisation of majoritic garnet. The starting mixture was prepared by mixing dried analytical grade oxides and carbonates. After grinding under ethanol in an agate mortar, the mixture was slowly decarbonated in air from 600 to 1000 °C and

reground before adding trace elements at ~50–500 ppm level using 1000 ppm atomic absorption standard solutions. The doped powder was then denitrified at 800 °C for about 2 h and was subsequently reduced in a controlled atmosphere furnace at 1000 °C for several hours at an oxygen fugacity about 2 log units below the fayalite–magnetite–quartz oxygen buffer.

Experiments were performed at 10, 15, and 17 GPa using 800- and 1500-ton Walker-type multi-anvil presses at the Geophysical Laboratory. The pressure scale was calibrated against the coesite–stishovite transformation at 1500 °C (Zhang et al., 1996) and the forsterite–wadsleyite transformation in $Fo_{92}$ at 1600 °C (Katsura et al., 2004). We estimate pressure uncertainties to be $\pm 0.5$ GPa. The starting mixture was contained in an unsealed rhenium capsule (~1.5 mm long prior to experiment) surrounded by a magnesia sleeve, a cylindrical rhenium heater and an outer zirconia sleeve as thermal insulator (Fig. 1). The octahedral pressure cell (MgO with 5% $Cr_2O_3$) with 10 mm edge length was compressed using 25 mm Toshiba tungsten carbide anvils with 5 mm truncations. Temperature was measured using type-C ($W_{26}Re$–$W_5Re$) thermocouples and was controlled automatically to within $\pm 2$ °C. The effect of pressure on the thermocouple electromotive force was ignored. The thermocouple was inserted axially above the rhenium capsule (Fig. 1). Given the dimensions of the sample chamber during heating (diameter × height = $250 \times 150$ μm), the temperature gradient across the sample in this set of experiments is estimated to be within 30 °C. This estimation is derived from the studies of Walter et al. (1995) and van Westrenen et al. (2003) on temperature distribution in multi-anvil assemblies. Each experiment was pressurised at room temperature at ~3 GPa/h, then raised at ~100 °C/min to the target temperature and held there for 45–150 min to approach chemical equilibrium. The experiment was quenched rapidly by switching off the power to the rhenium furnace and then decompressed gradually at ~3 GPa/h. The recovered pressure cell was mounted in Petropoxy-154 resin and polished longitudinally for optical and chemical analyses. Table 2 details run conditions and produced phase assemblages. The experimental approach followed here therefore contrasts with a number of previous experimental studies on mantle melting, where a large temperature gradient (>200 °C) existed across the sample and run durations were as short as a few minutes

**Table 1**
Composition of the starting mixture and comparison with model mantle compositions.

|  | This study | Pyrolite-model | CI-model |
|---|---|---|---|
| $SiO_2$ (wt.%) | 47.8 | 44.9 | 49.4 |
| $TiO_2$ | 0.21 | 0.20 | 0.16 |
| $Al_2O_3$ | 4.50 | 4.44 | 3.62 |
| $Cr_2O_3$ | 0.37 | 0.38 | 0.44 |
| $FeO^*$ | 8.00 | 8.03 | 7.93 |
| MgO | 35.0 | 37.7 | 34.8 |
| CaO | 3.50 | 3.54 | 2.87 |
| MnO | 0.15 | 0.14 | 0.13 |
| NiO | 0.22 | 0.25 | 0.25 |
| $Na_2O$ | 0.20 | 0.36 | 0.34 |
| $K_2O$ | 0.03 | 0.03 | 0.02 |
| Total | 100.0 | 100.2 | 100.5 |
| Molar Mg/Si | 1.09 | 1.25 | 1.05 |
| Molar Mg/[Mg + Fe] | 0.886 | 0.893 | 0.887 |

Pyrolite- and CI-model from McDonough and Sun (1995).
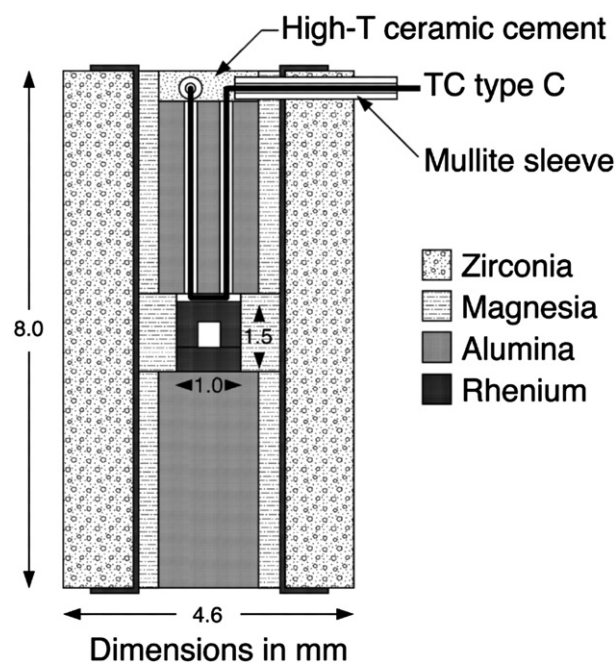


**Fig. 1.** Schematic cross-section of the 10 mm cell-assembly used in this study.

**Table 2**
Experimental conditions and run products.

| Run | P (GPa) | T (°C) | t (min) | Phase assemblage (wt.%) |
|---|---|---|---|---|
| LO540 | 17 | 2220 | 45 | Liq (75) + Maj (25) |
| M932 | 15 | 2110 | 150 | Liq (71) + Maj (20) + Ol (9) |
| M955 | 10 | 1975 | 120 | Liq (64) + Ol (19) + Maj (4) + Opx (13) |

Abbreviations: P, pressure; T, temperature; t, run duration; Liq, silicate melt; Maj, majoritic garnet; Ol, olivine; Opx, orthopyroxene. Phase abundances were calculated from mass balance considerations for the 5 major oxides (CaO, MgO, $Al_2O_3$, $SiO_2$ and FeO).

(e.g., Herzberg and Zhang, 1996; Kato et al., 1988; Takahashi and Scarfe, 1985; Trønnes et al., 1992).

Major element concentrations of the resulting phase assemblages were measured using a 5-spectrometer JEOL 8800 superprobe at the Geophysical Laboratory. Analytical conditions were 15 kV accelerating voltage and 30 nA beam current. Counting times were 30 s on peak and 15 s on background for Si, Ti, Al, Fe, Mg and Ca and 60 s on peak and 30 s on background for Cr, Mn, Ni, Na and K. Calibration standards were a basaltic glass (Si, Ti, Al, Fe, Ca and Na), diopside (Cr, Mg, Mn and Ni) and orthoclase (K). Minerals were analysed with a focused beam, whereas quenched melt areas were analysed with a rastering beam of ~40 $\mu m^2$ to average the compositions of fine-grained quench crystals and glass that compose the melt. Analyses were reduced using a ZAF correction routine. Trace element concentrations were determined by laser ablation–inductively coupled plasma-mass spectrometry (LA–ICP-MS) at the Department of Geology, University of Maryland. Concentrations of some trace elements of the 15 and 17 GPa runs were also measured by LA–ICP-MS at the Department of Earth Sciences, McGill University. The later results (not reported here except for Li and Rb) show good agreement with the data obtained at the University of Maryland. LA–ICP-MS analyses at the University of Maryland were performed using a frequency-quintupled Nd:YAG 213 nm laser (UP213 from New Wave Research) coupled to an Element 2 (Thermo Finnigan MAT) magnetic sector ICPMS. The ablation cell was flushed with 0.7 L/min He to enhance sensitivity. Laser ablation was operated using a 10–12 Hz frequency and, for majoritic garnet, in spot sampling mode with a 15–30 μm beam diameter and, for silicate liquids, in both spot and line sampling mode with a beam diameter of 15–40 μm. Background gas blanks were measured on all masses for ~25 s before laser ablation, total laser firing time was usually ~40 s for silicate melt analyses and ~10 s for majoritic garnet analyses. Concentration of Mn determined by electron microprobe was used as the internal standard for processing trace element data. The reference NIST 610 glass was used as calibration standard. Selected time-resolved spectra were processed off-line using a spreadsheet program (modified version of LAMTRACE by Simon E. Jackson) to apply background subtraction and calculate absolute trace element abundances. Variations in ablation yields were corrected by reference to Mn concentrations measured by electron microprobe. LA–ICP-MS analyses at McGill University were carried out using a New Wave UP213 laser ablation system coupled to a PerkinElmer ELAN 6100 DRC plus ICPMS. Raw data were reduced using GLITTER 4.0 and using Si as internal standard and NIST 610 as calibration standard. For both LA–ICP-MS systems, minimum detection limits for reported concentrations are calculated on the basis of 2 standard deviations above the background count rate. With the setup described above, repetitive analyses of the NIST 610 standard show that the analytical precision of both LA–ICP-MS systems is better than 3% for all measured elements. Accuracy was assessed by comparing observed and published contents of secondary silicate standards (NIST 612 and BCR-2g). Observed/published concentration ratios show that accuracy is better than 5% for all elements studied here except Ti, Yb, Zr, Y, Nb, Nd, Lu, Hf, Th (usually better than 10–15%), and Ta (30%).

# 3. Results

## 3.1. Phase relations

Phase relations in our experiments are in general agreement with previous observations on mantle phase relations at high pressures (e.g., Zhang and Herzberg, 1994). At 17 GPa and 2220 °C, majoritic garnet coexists with silicate liquid. At 15 GPa and 2110 °C, olivine and garnet are both present in the melting interval, with approximately the same position in the crystallisation sequence. At 10 GPa, olivine becomes the liquidus phase followed down temperature by majoritic garnet and orthopyroxene. To our knowledge, this is the first time that orthopyroxene has been observed above the solidus of peridotite at pressures greater than 7 GPa (as previously reported by Walter, 1998). We note, however, that orthopyroxene was previously reported at 9 GPa in the melting interval of a metal-free ordinary chondrite starting composition (Draper et al., 2003). The use of a silica-rich peridotite composition as starting composition and relatively oxidising conditions (Re-capsule) may have promoted crystallisation of orthopyroxene in our runs (Lesher et al., 2003). Fig. 2 shows backscattered electron images of the run products. At 17 GPa, garnet crystals are less than ~30 μm in diameter, making trace element analyses somewhat difficult but possible
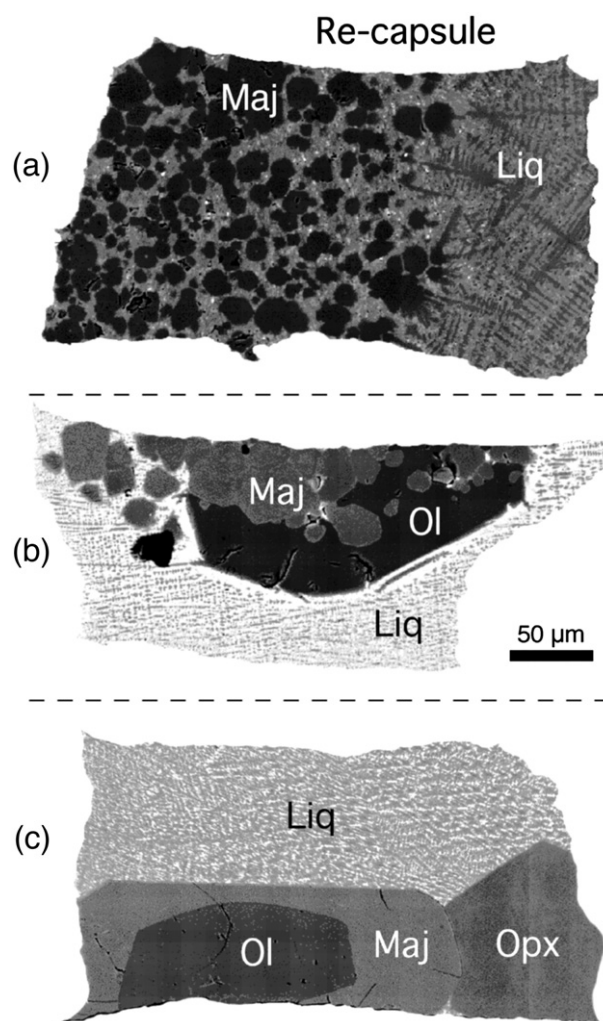


**Fig. 2.** Back-scattered electron images of run products at (a) 17 GPa and 2220 °C, (b) 15 GPa and 2110 °C, and (c) 10 GPa and 1975 °C. Abbreviations are: Maj, majoritic garnet; Liq, silicate liquid; Ol, olivine; Opx, orthopyroxene. Note that the liquid does not quench into a glass but is instead composed of quench crystals and glass.

for a LA–ICP-MS beam size on the order of ~15 μm. Crystals grew larger in our run at lower pressures (up to 50 μm) allowing the use of LA–ICP-MS beam size up to ~30 μm. Phase proportions were determined by least-square mass balance calculation of major elements (Ca, Mg, Al, Si and Fe). Results of the calculation together with experimental details are given in Table 2.

### 3.2. Major element composition

Major and trace element compositions of the run products are presented in Table 3. The composition of the quenched melt in each run is homogeneous throughout the entire charge and resembles the bulk composition due to high degrees of partial melting (about 70%). The melt contains slightly more FeO, CaO, $TiO_2$ and $Al_2O_3$ but less MgO at lower pressure–temperature conditions (Table 3). The silicate melt has an Mg# of 0.851, 0.867 and 0.885, respectively at 10, 15 and 17 GPa. Olivine, garnet and orthopyroxene contain less Fe than the melt, resulting in larger Mg# for these phases (~0.95). The major element composition of olivine crystals remains the same at both 10 and 15 GPa. In contrast, with increasing pressure, majoritic garnet becomes enriched in the $MgSiO_3$ component and depleted in Al and Cr. The number of Si atoms per formula unit is 3.14, 3.38 and 3.48 at 10, 15 and 17 GPa, respectively (Table 3), while the proportion of Mg in the Y-site calculated by stoichiometry increases from 7% at

10 GPa to 14% at 15 GPa and 16% at 17 GPa. The sum of Al and Cr atoms per formula unit (pfu, normalised to 12 oxygen atoms) is 1.67, 1.18 and 1.02 at 10, 15 and 17 GPa, respectively. As shown in Fig. 3, these variations are in excellent quantitative agreement with previous experimental works on subsolidus and melting phase relations of dry peridotite (Akaogi and Akimoto, 1979; Herzberg and Zhang, 1996; Irifune, 1987; Ito and Takahashi, 1987; Kato et al., 1988; Ohtani et al., 1986; Suzuki et al., 2000; Walter, 1998; Wang and Takahashi, 2000). Interestingly, at a fixed pressure, high- and low-temperature runs provide similar Si and Al + Cr (pfu) in majoritic garnet. This observation implies that, in peridotite-like composition, temperature has a relatively minor effect on majoritic garnet composition, in agreement with early results at 16 GPa by Kato et al. (1988) and conclusions reached by Collerson et al. (2010). This interpretation is however limited to pressures below ~22 GPa, i.e. outside the stability field of calcium and magnesium silicate perovskites, two minerals which form from the gradual breakdown of majoritic garnet (e.g., Hirose, 2002; Niyashima and Yagi, 2004; Wood, 2000). Experiments performed at pressures where majoritic garnet coexists with calcium or magnesium silicate perovskites reveal that the modal proportion and the majoritic content of garnet increase significantly with increasing temperature (e.g., Niyashima and Yagi, 2004). This is because the two perovskites become less stable at high temperature and dissolve into the garnet phase.

**Table 3**
Major and trace element compositions of the run products (by weight).

| Run | LO540 (17 GPa, 2220 °C, 45 min) | | | M932 (15 GPa, 2110 °C, 150 min) | | | | M955 (10 GPa, 1975 °C, 120 min) | | | | |
|---|---|---|---|---|---|---|---|---|---|---|---|---|
| Phase, D | Maj | Liq | D Maj/Liq | Maj | Ol | Liq | D Maj/Liq | Maj | Ol | Opx | Liq | D Maj/Liq |
| EPMA | N = 22 | N = 53 | | N = 12 | N = 6 | N = 28 | | N = 17 | N = 14 | N = 5 | N = 20 | |
| SiO₂ (%) | 51.2 (2) | 46.6 (8) | 1.10 (2) | 49.8 (3) | 41.8 (1) | 48.5 (2) | 1.03 (1) | 45.9 (2) | 41.7 (3) | 57.1 (3) | 47.9 (5) | 0.96 (1) |
| TiO₂ (%) | 0.06 (1) | 0.26 (1) | 0.22 (2) | 0.06 (1) | <0.04 | 0.31 (1) | 0.20 (2) | 0.08 (0) | <0.04 | 0.02 (1) | 0.40 (6) | 0.21 (3) |
| Al₂O₃ (%) | 12.3 (4) | 2.25 (21) | 5.44 (53) | 14.2 (3) | 0.17 (1) | 2.28 (6) | 6.23 (21) | 19.6 (2) | 0.27 (1) | 2.44 (12) | 5.18 (11) | 3.86 (9) |
| Cr₂O₃ (%) | 0.61 (2) | 0.29 (2) | 2.11 (16) | 0.85 (4) | 0.07 (1) | 0.26 (1) | 3.31 (18) | 1.64 (7) | 0.13 (1) | 0.27 (2) | 0.35 (1) | 4.62 (21) |
| FeO* (%) | 2.64 (4) | 8.69 (42) | 0.30 (2) | 2.92 (8) | 4.31 (16) | 9.24 (7) | 0.32 (1) | 3.34 (10) | 4.50 (18) | 3.44 (25) | 9.45 (41) | 0.35 (2) |
| MgO (%) | 31.7 (1) | 37.6 (6) | 0.84 (1) | 31.2 (3) | 54.1 (1) | 33.9 (5) | 0.92 (2) | 28.0 (2) | 53.8 (3) | 35.0 (6) | 30.2 (3) | 0.93 (1) |
| CaO (%) | 1.81 (4) | 4.24 (26) | 0.43 (3) | 1.67 (7) | 0.13 (1) | 5.16 (12) | 0.32 (2) | 2.12 (7) | 0.15 (1) | 1.49 (20) | 6.09 (11) | 0.34 (1) |
| MnO (ppm) | 835 (51) | 1708 (86) | 0.49 (4) | 865 (45) | 655 (102) | 1785 (73) | 0.48 (3) | 1111 (61) | 763 (42) | 888 (81) | 1998 (77) | 0.56 (4) |
| NiO (ppm) | <300 | 929 (107) | <0.33 | <300 | 1208 (136) | 788 (78) | <0.30 | <300 | 1184 (131) | 602 (67) | 767 (65) | <0.40 |
| Na₂O (ppm) | 421 (35) | 2326 (145) | 0.18 (2) | 375 (50) | <202 | 3605 (154) | 0.10 (1) | 187 (30) | <202 | 1532 (112) | 4244 (123) | 0.044 (7) |
| K₂O (ppm) | <170 | 284 (24) | <0.58 | <170 | 183 (25) | 290 (33) | <0.56 | <170 | 169 (23) | <170 | 586 (41) | <0.32 |
| Total (%) | 100.3 | 100.3 | | 100.9 | 100.8 | 100.3 | | 100.9 | 100.8 | 100.1 | 100.2 | |
| Mg/(Mg + Fe) | 0.955 | 0.885 | | 0.950 | 0.957 | 0.867 | | 0.937 | 0.955 | 0.948 | 0.851 | |
| K^Fe/Mg | 0.36 | | | 0.34 | 0.29 | | | 0.38 | 0.27 | 0.31 | | |
| Si (12 O) | 3.48 | | | 3.38 | | | | 3.14 | | | | |
| Al + Cr (12 O) | 1.02 | | | 1.18 | | | | 1.67 | | | | |
| | | | | | | | | | | | | |
| LA–ICP-MS | N = 4 | N = 5 | | N = 8 | N = 8 | | | N = 6 | | | N = 7 | |
| CaO (%) | 1.72 (17) | 4.24 (31) | 0.41 (5) | 1.49 (19) | 4.5 (1) | 0.33 (4) | | 1.65 (2) | | | 5.67 (24) | 0.29 (1) |
| Li (ppm) | 49 (16) | 625 (67) | 0.078 (27) | 37 (5) | 583 (40) | 0.063 (10) | | | | | | |
| Sc (ppm) | 48.5 (25) | 50 (4) | 0.96 (10) | 61 (4) | 49 (3) | 1.25 (11) | | 101 (9) | | | 66 (3) | 1.53 (16) |
| Ti (ppm) | 310 (59) | 1448 (68) | 0.21 (4) | 281 (29) | 1549 (60) | 0.18 (2) | | 389 (47) | | | 1983 (92) | 0.20 (3) |
| Rb (ppm) | <4.6 | 122 (22) | <0.04 | <4.7 | 51 (24) | <0.092 | | | | | | |
| Sr (ppm) | <2.4 | 61 (7) | <0.04 | <0.70 | 61 (5) | <0.011 | | <2.0 | | | 106 (14) | <0.019 |
| Y (ppm) | 39.6 (15) | 97 (5) | 0.41 (3) | 51 (5) | 112 (6) | 0.45 (5) | | 88 (10) | | | 133 (5) | 0.67 (8) |
| Zr (ppm) | 20.3 (52) | 138 (10) | 0.15 (4) | 25 (6) | 162 (32) | 0.15 (5) | | 45 (8) | | | 573 (19) | 0.078 (14) |
| Nb (ppm) | 1.9 (14) | 51 (6) | 0.037 (29) | 0.7 (2) | 56 (3) | 0.012 (3) | | 2.0 (8) | | | 78 (1) | 0.026 (10) |
| Ba (ppm) | <2.1 | 54 (5) | <0.04 | <2.9 | 63 (13) | <0.046 | | <2.0 | | | 119 (3) | <0.017 |
| La (ppm) | <0.6 | 65 (9) | <0.0087 | <0.71 | 76 (3) | <0.0094 | | <0.88 | | | 104 (5) | <0.0085 |
| Ce (ppm) | <1.1 | 53 (8) | <0.021 | <0.64 | 60 (1) | <0.011 | | <1.2 | | | 89 (3) | <0.013 |
| Nd (ppm) | 1.3 | 55 (5) | 0.024 (15) | 1.8 (8) | 61 (3) | 0.029 (13) | | 1.2 (7) | | | 90 (4) | 0.013 (8) |
| Sm (ppm) | 5.8 (10) | 56 (7) | 0.10 (2) | 4.5 (8) | 66 (3) | 0.068 (13) | | 12 (2) | | | 95 (4) | 0.12 (2) |
| Lu (ppm) | 40.8 (18) | 43 (5) | 0.94 (11) | 47 (4) | 43 (3) | 1.09 (12) | | 110 (11) | | | 71 (2) | 1.54 (16) |
| Hf (ppm) | 10.4 (11) | 48 (5) | 0.21 (3) | 12 (2) | 51 (3) | 0.23 (4) | | 21 (4) | | | 87 (3) | 0.25 (4) |
| Ta (ppm) | 1.3 (12) | 41 (6) | 0.031 (29) | 0.6 (5) | 43 (2) | 0.014 (12) | | 1.4 (6) | | | 72 (2) | 0.020 (8) |
| Th (ppm) | 1.0 (7) | 48 (5) | 0.021 (15) | 0.6 (1) | 52 (5) | 0.012 (11) | | 1.7 (10) | | | 88 (4) | 0.020 (12) |
| U (ppm) | 2.2 (15) | 49 (5) | 0.045 (30) | 0.8 (3) | 48 (2) | 0.016 (6) | | 2.6 (10) | | | 88 (5) | 0.030 (12) |

Numbers in parentheses are 2 standard errors in terms of least digits cited.
Li and Rb contents were measured by LA–ICP-MS at McGill University. All other LA–ICP-MS measurements were made at the University of Maryland.
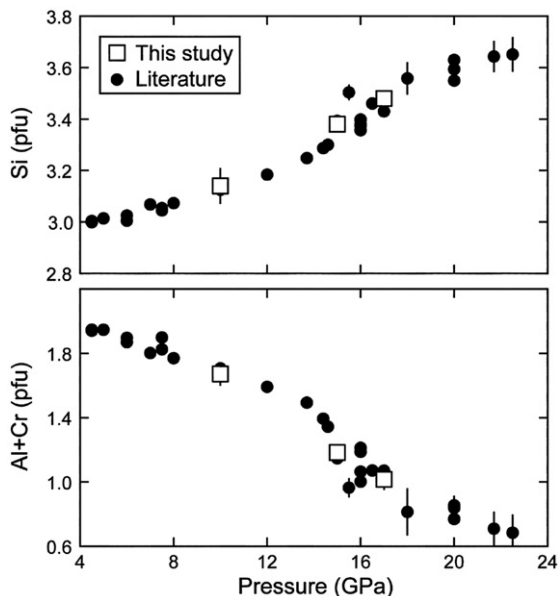
**Fig. 3.** Number of Si and Al + Cr atoms in majoritic garnet per formula unit (pfu) calculated on the basis of 12 oxygen atoms as a function of pressure. Literature data are for subsolidus and melting experiments on dry peridotite from Akaogi and Akimoto (1979), Herzberg and Zhang (1996), Irifune (1987), Ito and Takahashi (1987), Kato et al. (1988), Ohtani et al. (1986), Suzuki et al. (2000), Walter (1998) and Wang and Takahashi (2000).

Given its strong dependence on pressure (e.g., Akaogi and Akimoto, 1979; Irifune, 1987), the major element composition of majoritic garnet has been used as an empirical geobarometer (e.g., Collerson et al., 2000; 2010; Keshav and Sen, 2001; Stachel et al., 2000). Using atomic proportions of Al + Cr and Si as pressure indicators and using the reference study of Irifune (1987), we derive pressures of about 10.5 and 15.1 for runs M932 and M955, i.e. in good agreement with the expected calibrated values of 10 and 15 GPa. Using the geobarometer of Collerson et al. (2000), the same values of Al + Cr and Si lead to an underestimation of the actual run pressures by about 15%. The recently updated version of their geobarometer (Collerson et al., 2010), which now takes into account Ti and Na substitutions, also underestimates the actual run pressures by about 15%, a value that is within uncertainties of the empirical geobarometer. The slight discrepancy between our data and the geobarometers of Collerson and coworkers almost certainly arises from the geobarometer calibration itself, which is partly based on experiments performed with large temperature gradients, short run duration, non-peridotitic starting compositions, and experiments which were performed in the stability field of calcium and magnesium silicate perovskites (e.g., Herzberg and Zhang, 1996; Hirose, 2002; Litasov and Ohtani, 2003).

### 3.3. Mineral–melt partitioning

Partition coefficients ($D_i$) are reported in Table 3. $D_i$ is defined as the ratio of the weight fraction of element i in the mineral over the weight fraction of the same element in the melt. Partition coefficients for all elements investigated in this study including trace elements are plotted in Fig. 4a according to their charge and size. All three experiments show a well-defined distribution pattern with, in general, a higher degree of compatibility for smaller cations at a given charge. Most of the elements are incompatible ($D<1$) in majoritic garnet with the exception of Si, Al, Cr, Sc and Lu. Partition coefficients show a considerable range in magnitude, from ~6 for $D_{Al}$ to less than 0.01 for example for $D_{Sr}$. In particular, REE display a wide range of partition coefficients, $D_{Lu}$ (~1) being at least 100 times higher than $D_{La}$ (<0.01). Heat producing

elements U and Th are highly incompatible in majoritic garnet with mean D values of about 0.02. As shown in Fig. 4b, our results are in broad agreement with previous high-pressure studies. The overall pattern of our data is best matched by the data from Corgne and Wood (2004) and Walter et al. (2004) at 25 and 23.5 GPa. Results from Ohtani et al. (1989) at 16 GPa show more discrepancies. Run durations may have been too short (~4 min) for attainment of chemical equilibrium in the experiments of Ohtani et al. (1989). The value derived by Walter et al. (2004) for Nb (~0.002) remains at odd with the values (~0.01–0.04) derived in this study and in Corgne and Wood (2004). The latter values are similar to values obtained for Ta, an element that has a geochemical affinity with Nb given similarities in charge (5+) and size.

## 4. Discussion

### 4.1. Crystal lattice strain

Experimental work on solid–melt partitioning of cations (Blundy and Wood, 1994; Wood and Blundy, 2001) has quantified the effects of ionic radius and charge on partitioning behaviour. Blundy and Wood (1994) showed, following elastic strain theory (Brice, 1975), that the solid–liquid partition coefficient ($D_i$) of cation i of radius $r_i$ can be calculated from that of an hypothetical cation ($D_o$) of the same charge, which enters the site without strain following:

$$D_i = D_o \exp\left(\frac{-4\pi E_s N_A}{RT}\left(\frac{r_o}{2}(r_o-r_i)^2 - \frac{1}{3}(r_o-r_i)^3\right)\right). \tag{1}$$

In Eq. (1), $r_o$ is the effective radius of the site, $N_A$ is Avogadro's number and $E_S$ is the effective Young's Modulus of the site. Eq. (1) give a physical meaning to the near-parabolic relationship first observed by Onuma et al. (1968) between log $D_i$ and radius for cations of fixed charge. The peak of the parabola corresponds to $r_o$ and $D_o$, while the tightness of the parabola depends on the 'stiffness' of the site represented by $E_s$.

Majorite-rich garnets from the mantle have cubic symmetry with the general structural formula $X_3Y_2Z_3O_{12}$, where the X-, Y- and Z-positions are dodecahedral, octahedral and tetragonal cation sites, respectively (e.g., Heinemann et al., 1997). In agreement with cation size and stoichiometry, crystallographic and spectroscopic considerations (e.g., Heinemann et al., 1997; McCammon and Ross, 2003; Smyth and Bish, 1988) indicate that in majoritic garnet (i) Si is present in both Y- and Z-sites, (ii) Mg and $Fe^{2+}$ occupies the X- and Y-sites but with only a minor proportion in the Y-site, (iii) Al and $Fe^{3+}$ occupy almost exclusively the Y-site, and (iv) Ca occupies predominantly the X-site. Partition coefficients reported here at 10, 15 and 17 GPa for a suite of isovalent cations entering the X-site exhibit the near-parabolic dependence on ionic radius predicted from Eq. (1). Fig. 5 presents the partitioning 'parabolas' derived from our 17 GPa data. Similar dependences (not shown here) were also obtained at 10 and 15 GPa (this study) and at 25 GPa (Corgne and Wood, 2004). These results underline the important contribution made by the crystal structure to the control of trace element partitioning. As previously found, $E_s$ increases and $r_o$ decreases with increasing charge of the cation incorporated at the X-site (Fig. 5). Furthermore, as observed by Corgne and Wood (2004), Mn does not fit the trend predicted from the elastic strain model applied to Ca, Mg and Sr. Since $Mn^{2+}$ does not have crystal field stabilisation energy with its $d^5$ high-spin electronic configuration, the misfit might be attributed to the presence of $Mn^{3+}$, which is about 0.1 Å smaller than $Mn^{2+}$ and is sensitive to crystal field effects.

### 4.2. Effect of pressure on partitioning

In the shallow mantle, garnets are enriched in the pyrope component ($Mg_3Al_2Si_3O_{12}$). They become more enriched in the majorite
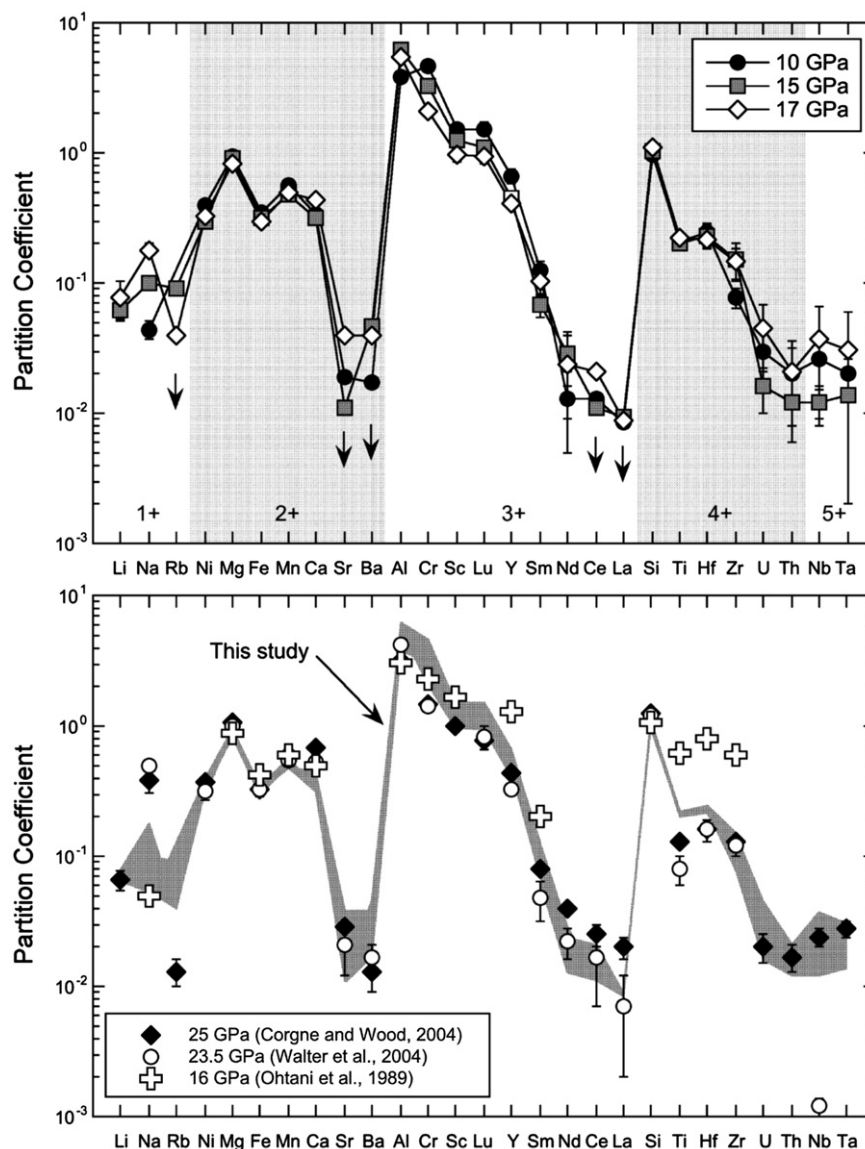
**Fig. 4.** Majoritic garnet–melt partition coefficients ordered according to cationic charge and size. (top) Data from this study. Upper bounds are shown for Rb, Sr, Ba, Nd, Ce and La as indicated by the downward-pointing arrows; (bottom) Comparison of data from this study (in grey) with high-pressure literature data from Corgne and Wood (2004), Ohtani et al. (1989) and Walter et al. (2004).

component at greater depths as pressure and temperature increase (Fig. 3). As a result, trace element partitioning is likely to be sensitive to variations in pressure and temperature as a consequence of changes in crystal lattice strain.

Partition coefficients for major and minor elements are reported as a function of pressure in Fig. 6 together with data for dry peridotite compositions from the literature (Corgne and Wood, 2004; Herzberg and Zhang, 1996; Ito and Takahashi, 1987; Litasov and Ohtani, 2003; Ohtani et al., 1989; Suzuki et al., 2000; Trønnes and Frost, 2002; Trønnes et al., 1992; Walter, 1998; Walter et al., 2004; Wang and Takahashi, 2000). $D_{Si}$ increases with increasing pressure. This is related to the increased solubility of majorite component in garnet at higher pressure. $D_{Mg}$ remains relatively constant between 0.9 and 1.0. Some of the scatter is linked to the presence of olivine or ferropericlase (Mg-rich minerals) coexisting with majoritic garnet in the melting interval, which leads to lesser Mg in the melt, and hence higher $D_{Mg}$. $D_{Fe}$ averages ~0.4 in the 5–25 GPa range with a slight decrease with increasing pressure. Like $D_{Mg}$ and $D_{Fe}$, $D_{Mn}$ is not significantly affected by variations of pressure, with values

ranging between 0.5 and 0.7. $D_{Ca}$ is approximately constant (~0.4) up to 20 GPa and increases up to ~0.7 at 25 GPa. $D_{Al}$ increases from ~3 at 5 GPa to ~5 at 15 GPa and then decreases to ~3 at 25 GPa, reflecting variations in both melt and garnet compositions. Melt Al content decreases up to ~15 GPa and remains constant at higher pressures, while garnet Al content remains approximately constant up to ~10 GPa and then decreases with increasing pressure. Similar observations were made by Herzberg and Zhang (1996). Fig. 6 shows that there is a continuous drop of $D_{Cr}$ with pressure, from about 3.5 at 5 GPa to 1.5 at 25 GPa. $D_{Na}$ increases by about an order of magnitude from 5 (~0.05) to 25 GPa (~0.5), reflecting the stabilisation of Na-rich garnet at higher pressure (Gasparik, 1990). One possibility for such stabilisation relates to the Na substitution mechanism in majorite (Ono and Yasuda, 1996). The incorporation of Na in the X-site of majoritic garnet creates a charge deficit, since the X-site is normally occupied by divalent cations. At higher pressure, as more $Si^{4+}$ substitute for $Al^{3+}$ in the Y-site, charge balancing of Na defects should be more readily achieved (Irifune et al., 1989). Therefore, Na solubility should increase with increasing pressure. Another possibility suggested
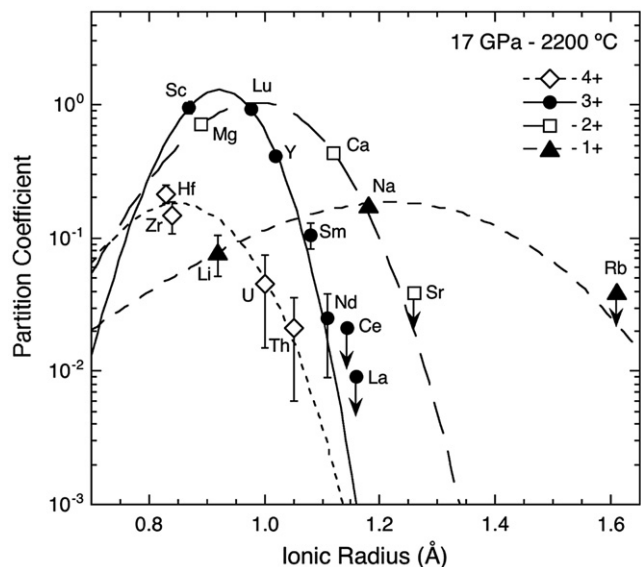
**Fig. 5.** Partitioning of elements entering the X-site of majoritic garnet plotted as a function of ionic radius. Near-parabolic dependences are obtained for isovalent cations as predicted by the lattice strain model of Blundy and Wood (1994). Upper bounds are shown for Ce, La, Sr and Rb (indicated by the arrows). All cations shown here are assumed to enter only the X-site, with the exception of Mg, which also enters the Y-site. $D_{Mg}$ for the X-site was calculated by stoichiometry.

by Suzuki et al. (2000) is that, because of its greater compressibility than that of divalent cations, Na would enter more readily in the crystal lattice of garnet as it becomes more majoritic.

Among the trace elements, trivalent cations are most affected by variations in pressure. Other trace elements do not show systematic changes with pressure as previously observed by Draper et al. (2003). Fig. 7 presents a series of partitioning parabolas for trivalent cations entering the X-site. Our data at 10–17 GPa are compared with data at 3 GPa from van Westrenen et al. (2000a) in the CaO-MgO-Al$_2$O$_3$-SiO$_2$-FeO system (Py$_{78}$Gr$_{19}$Alm$_9$ garnet with Mg# of 0.89), with data from Draper et al. (2003) obtained at 9 GPa on a ordinary chondrite composition (Py$_{80}$Gr$_{17}$Alm$_3$ garnet with Mg# of 0.83), with data from Walter et al. (2004) obtained at 23.5 GPa on a fertile peridotite composition (garnet Mg# of 0.95), and with data from Corgne and Wood (2004) at 25 GPa on an Al-, Fe-rich peridotite composition (garnet Mg# of 0.89). As noted by Draper et al. (2003) in the 5–9 GPa pressure range, $D_o^{3+}$ for the X-site decreases with increasing pressure, i.e. with increasing majorite component. $D_o^{3+}$ decreases by about an order of magnitude from about 8 to 0.8 over the 3–25 GPa pressure range. Furthermore, although there are relatively large uncertainties in D values for light REE, it appears that an increase of pressure results in more open parabolas, corresponding to lower values of Young's modulus ($E_X^{3+}$). In other words, the X-site becomes 'softer', i.e. more elastic with increasing pressure. The decrease of $D^{3+}$ with pressure may be seen as a consequence of the increasing solubility of Si in garnet. In detail, since both the incorporation of Si in the Y-site and the incorporation of trivalent cations in the X-site create charge excess, one can envisage that the mechanisms of charge compensation are interfering, resulting in the negative correlation between $D_o^{3+}$ and $D_{Si}$. A possibility mentioned above is that the substitution of Si for Al in the Y-site is coupled to the substitution of Na for Mg- or Ca- in the X-site. However, the mismatch between the amount of Si present in the Y-site (0.13–0.48 atoms pfu) and the amount of Na incorporated in the X-site (<0.01 atoms pfu) indicates that Na–Si coupled substitution is not sufficient to balance all Si atoms in the Y-site. Indeed, most of the charge balancing is made through the incorporation of Mg in the Y-site. Regarding REE substitution, spectroscopic studies have shown that REE are exclusively incorporated in the X-site of garnets as expected from size consideration (e.g., Quartieri et al., 1999). Charge compensation could take place via

divalent (Mg, Fe$^{2+}$) substitution for Al in the Y-site, like for Si incorporation in the Y-site. In that case, there would be a direct competition between Si and REE partitioning. Compensation could also occur through Al substitution for Si in the Z-site, or Mg- and Ca-vacancy formation in the X-site. These other two mechanisms could also interact indirectly with the coupled incorporation of Mg–Si in the Y-site and potentially explain the negative correlation between $D_{Si}$ and $D_o^{3+}$. Further work on majoritic garnet including atomistic simulations like the one performed by van Westrenen et al. (2000b) and Corgne et al. (2003) should help resolve this question.

### 4.3. Effect of composition on partitioning

As shown in Fig. 7, a small discrepancy exists between the results of Corgne and Wood (2004) and those of Walter et al. (2004) obtained at 25 and 23.5 GPa respectively. Considering the influence of pressure (or Si-content of garnet) on $D_o^{3+}$, one would expect the two parabolas to be inverted (i.e. $D_o^{3+}$(25 GPa)<$D_o^{3+}$(23.5 GPa)). Although part of the discrepancy may be related to experimental and analytical artefacts, additional factors such as bulk composition may have played a role. In comparison to the study of Walter et al. (2004), Corgne and Wood (2004) used a peridotite composition enriched in Fe, with a bulk Mg# 4% lower (~0.84). van Westrenen et al. (2000a) have shown that the addition of significant amount of Fe$^{2+}$ in the starting composition, and in particular in the garnet lattice, has only a minor effect on REE partitioning. Since the lattice parameters $E_X^{3+}$, $D_o^{3+}$ and $r_o^{3+}$ decrease slightly with increasing the proportion of almandine component, the data from Corgne and Wood (2004) 'corrected' for Fe should plot even higher in Fig. 7, leading to a larger discrepancy with the data of Walter et al. (2004). Another potential factor to consider is oxygen fugacity. Corgne and Wood (2004) used a Re-capsule, whereas Walter et al. (2004) used a graphite capsule, implying more reducing conditions in the latter study. Therefore, one can speculate that, in the experiments of Corgne and Wood (2004), majoritic garnet contains a significant amount of the andradite component (Ca$_3$Fe$^{3+}_2$Si$_3$O$_{12}$). Since andradite has the largest X-site of all garnet end-members (Smyth and Bish, 1988), partitioning parabola in andradite-rich garnet should be shifted to higher $r_o$ values. In other words, elements located on the right hand side of the partitioning parabola like REE should have higher partition coefficients in andradite-rich garnet. This may explain part of the discrepancy between the results of Corgne and Wood (2004) and those of Walter et al. (2004).

As discussed by van Westrenen et al. (2000b), melt composition is a potential controlling factor on garnet–melt partitioning. Indeed, the amount of energy associated with the incorporation of a given cation, and accordingly the partition coefficient of the cation, will depend on melt structural environment. In theory, the stronger the chemical bonds between the cation of interest and neighbouring elements, the lower the partition coefficient. Unfortunately, the lack of systematic experimental data does not allow us to estimate the contribution of melt relative to that of crystal structure.

### 4.4. Predictive model refinement

In the last decade, van Westrenen and coworkers have developed predictive models for the partitioning of REE, Sc and Y between garnet and anhydrous silicate melts (Draper and van Westrenen, 2007; van Westrenen and Draper, 2007; van Westrenen et al., 2001). High-pressure data for majoritic garnet were integrated in the last update of the model to extend the pressure range of its application from about 7 GPa to 25 GPa, i.e. over the entire stability field of garnet. However, only two studies at 23–25 GPa (Corgne and Wood, 2004; Walter et al., 2004) were available at the time to constrain the new model above 9 GPa, leaving a large gap without partitioning data between 9 and 23 GPa. Our data at 10, 15 and 17 GPa can thus be used to evaluate with more precision the progressive enrichment of garnet in majorite
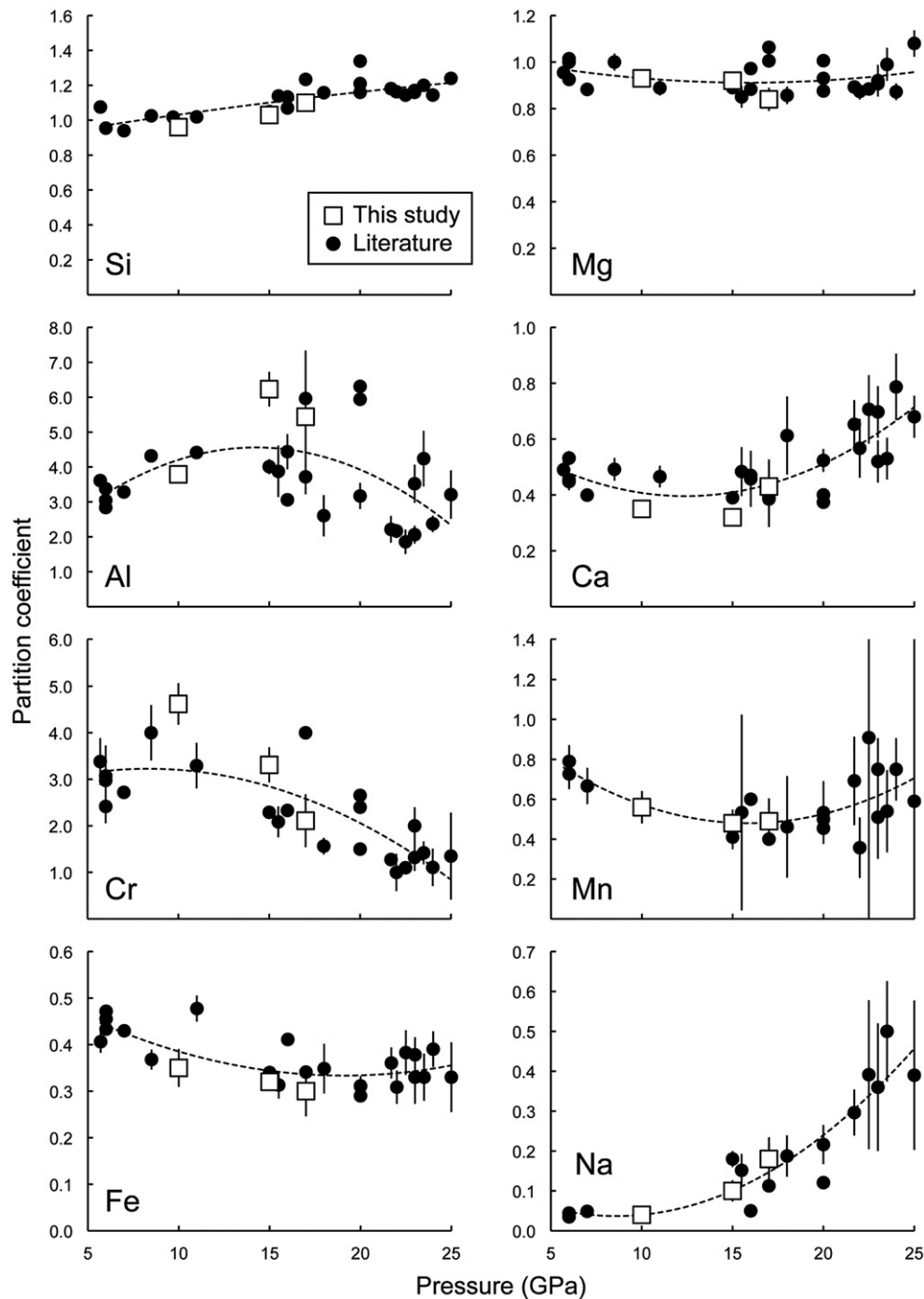
**Fig. 6.** Majoritic garnet–melt partitioning of major and minor elements as a function of pressure. Solid symbols are literature data from Corgne and Wood (2004), Herzberg and Zhang (1996), Ito and Takahashi (1987), Litasov and Ohtani (2003), Ohtani et al. (1989), Suzuki et al. (2000), Trønnes and Frost (2002), Trønnes et al. (1992), Walter (1998), Walter et al. (2004) and Wang and Takahashi (2000). Error bars are one standard deviation. Dashed lines are second-order polynomial best fits to the entire set of data.

component, and refine the predictive model proposed by van Westrenen and Draper (2007). As shown in Fig. 8, predicted partitioning parabolas closely match the experimental data reported here, if one considers the predictive model using an empirical determination of $D_0$ (Draper and van Westrenen, 2007). The other version of the model with $D_0$ derived on thermodynamic grounds (van Westrenen and Draper, 2007) underestimates the partition coefficients by a factor of about 2. Our data therefore suggest that the volume change of the partitioning reaction is pressure dependent, contrary to the hypothesis taken by van Westrenen and Draper (2007) in the absence of reliable experimental data in the 10–23 GPa interval. The pressure dependence of the volume change is in agreement with previous prediction for

garnet–melt partitioning of REE under hydrous compositions (Wood and Blundy, 2002). Using our data to refine the predictive model given in Eq. (18) of van Westrenen and Draper (2007), we obtain the following equation for $D_0$:

$$D_0 = \exp\left(\frac{389500 + 7850 \cdot P - 110 \cdot P^2}{RT}\right)/(\gamma_{Fe}D_{Fe})^2 \qquad (2)$$

where P is the pressure in GPa, T the temperature in K, R the gas constant and $\gamma_{Fe}$ and $D_{Fe}$ are the activity coefficient of Fe in garnet and Fe garnet–melt partition coefficient, respectively. As shown in Fig. 8, the
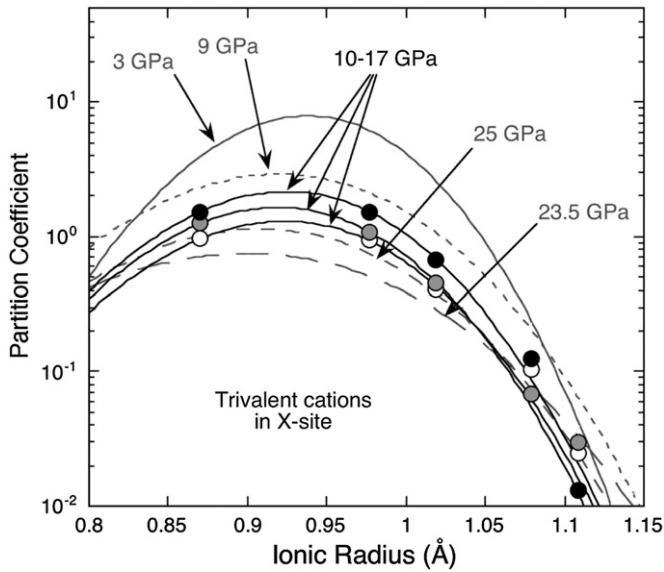
**Fig. 7.** Lattice strain parabolas for trivalent cations (Sc, Lu, Y, Sm, Nd) entering the X-site of majoritic garnet. References are: van Westrenen et al. (2000a), 3 GPa; Draper et al. (2003), 9 GPa; this study, 10–17 GPa; Walter et al. (2004), 23.5 GPa; Corgne and Wood (2004), 25 GPa. Lattice strain fit parameters for our data are: $E_X^{3+} = 646(53)$ GPa, $r_0^{3+} = 0.924(1)$ Å, $D_0^{3+} = 2.16(8)$ at 10 GPa (values in parentheses are one standard deviation); $E_X^{3+} = 683(30)$ GPa, $r_0^{3+} = 0.919(1)$ Å, $D_0^{3+} = 1.65(3)$ at 15 GPa; $E_X^{3+} = 667(108)$ GPa, $r_0^{3+} = 0.923(3)$ Å, $D_0^{3+} = 1.31(9)$ at 17 GPa.

refined equation together with Eqs. (3) and (6) of van Westrenen and Draper (2007) for the description of $r_0^{3+}$ and $E_X^{3+}$ now provide a better description of the experimental data, with a level of precision matching that of the predictive model with empirical determination of $D_0$ (Draper and van Westrenen, 2007).
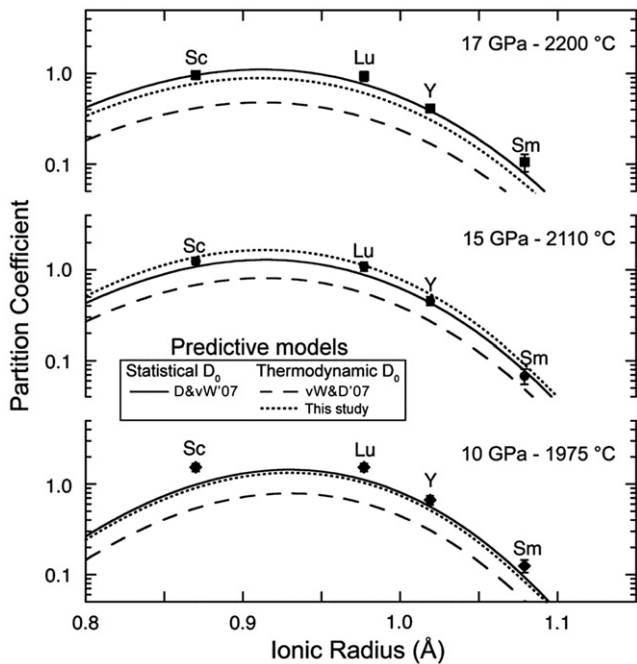


**Fig. 8.** Comparison between experimental data from this study (closed symbols) and predictive models from this study and that of Draper and van Westrenen (2007) (D&vW'07) and van Westrenen and Draper (2007) (vW&D'07). The model using a statistical approach to estimate $D_0$ and our refined model using a thermodynamic approach provide the best match to the data.

## 5. Applications

In the forthcoming sections, we use the partitioning data presented here to discuss processes that may involve partial melting or crystallisation in the presence of majoritic garnet: (i) the generation of Archean Al-depleted komatiites, (ii) the petrogenesis of garnet-bearing transition zone diamonds and (iii) the crystallisation of a putative Martian magma ocean.

### 5.1. Generation of Archean Al-depleted komatiites

Komatiites are spinifex-textured ultramafic rocks with high MgO contents that erupted from early Archean to Cretaceous. As such, they may provide a record of the compositional and thermal evolution of the Earth's mantle. Experimental works have proposed that komatiitic magmas can be generated by melting of peridotite in the 3–15 GPa pressure range (e.g. Gudfinnsson and Presnall, 1996; Herzberg, 1995; Takahashi and Scarfe, 1985; Walter, 1998). It has also been suggested that komatiites in Archean belts were generated at the highest pressures and temperatures (e.g. Herzberg, 1992, 1995; Takahashi, 1990; Walter, 1998). Some ~3.5 Ga old komatiites are depleted in Al and heavy REE, a signature attributed to garnet fractionation during their melt generation event (e.g. Arndt, 1986; Blichert-Toft and Arndt, 1999; Green, 1975; Jahn et al., 1982; Sun and Nesbitt, 1978). Al-depleted komatiites (ADK) have subchondritic Al/Ti and Yb/Gd ratios.

Using a batch melting equation and partition coefficients from this study, we have modelled the Al/Ti and Gd/Yb ratios in the melt when majoritic garnet is left in the residue during partial melting between 15 and 10 GPa. Using partitioning data from Walter et al. (2004) and the predictive model of van Westrenen et al. (2001), we also modelled melting paths at 23.5 and 4.5 GPa, respectively. The calculation assumes reasonably that majoritic garnet is the only major host phase for REE in the deep asthenosphere. It is noted that Ca-perovskite, which is stable in the mantle above ~21 GPa, is also a major host phase for REE (e.g., Corgne and Wood, 2002, 2005). Its effect on the melting path calculated at 23.5 GPa using the data of Walter et al. (2004) is negligible, however, except for very small degree melts since it disappears within the first few percents of partial melting of peridotite (Trønnes and Frost, 2002).

Results of these calculations are shown in Fig. 9. They suggest that partial melting of anhydrous peridotite in the transition zone (>13 GPa) in the presence of residual majoritic garnet is not the mechanism responsible for the generation of Archean ADK. However, a similar mechanism at lower pressures would be more appropriate. The compositional field of Archean ADK from Barberton (South Africa) is bracketed by melting paths at ~12 and ~6 GPa, with respectively up to ~35 and ~20% of residual garnet (Fig. 9). This pressure range overlaps slightly the pressure estimate (8–10 GPa) of Herzberg (1992) and Walter (1998) obtained on the basis of major element fractionation.

In the last 20 years, evidence has been presented for a possible important role of water in komatiite generation (e.g., Grove et al., 1994; Parman et al., 1997). Considering this possibility, Inoue et al. (2000) performed water-saturated garnet–melt partitioning experiments. Their results (not shown in Fig. 9 for clarity) suggest that a pressure range between 5.5 and 16 GPa and a percentage of garnet removal less than 25% are appropriate conditions for the generation of ADK. These values being similar to the ones we derived here for anhydrous conditions, the addition of water to the system would appear to play only a minor role in ADK genesis.

### 5.2. Speculations on the formation of majoritic garnet-bearing diamonds

The presence of majoritic garnet inclusions in diamonds is evidence for diamond formation within the transition zone (e.g., Moore and Gurney, 1985). The paragenesis of mineral inclusions in transition zone diamonds is almost exclusively eclogitic, with majoritic garnet
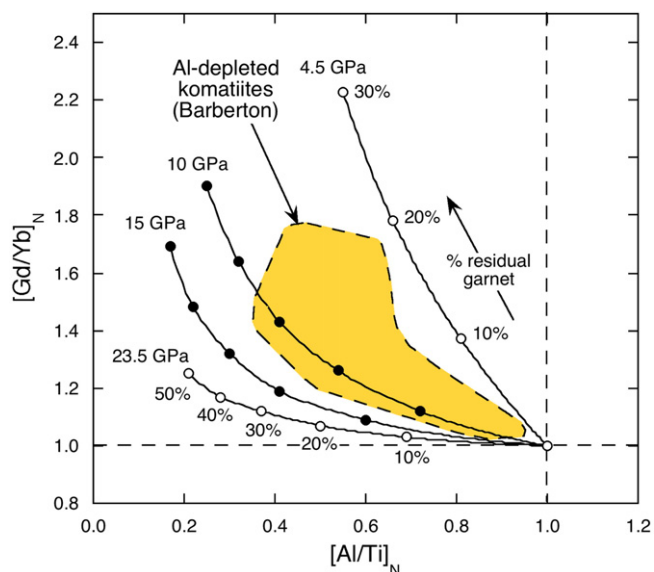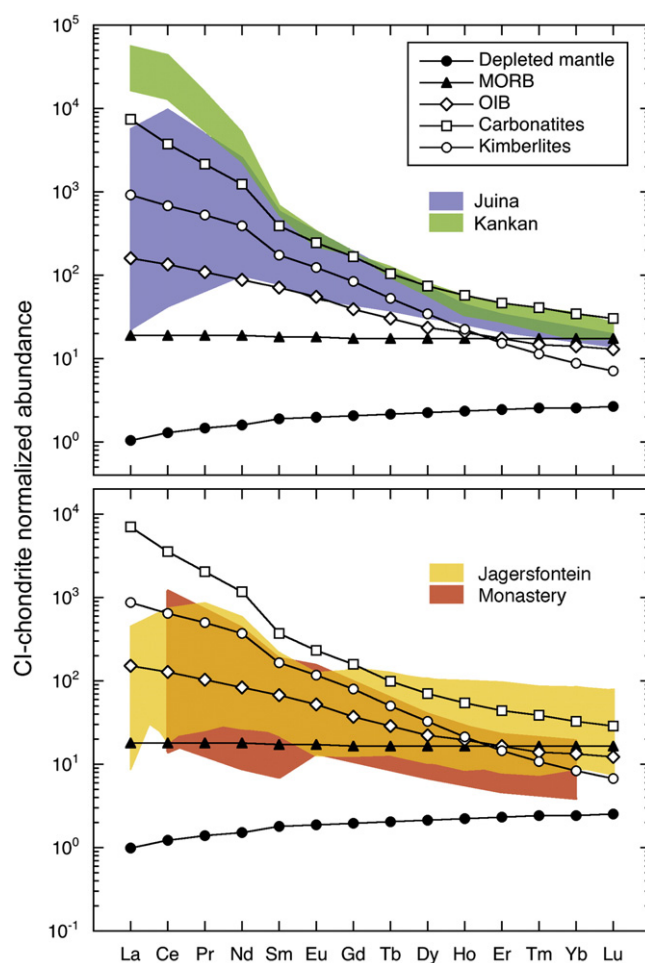
**Fig. 9.** Evolution of chondrite-normalised Gd/Yb and Al/Ti ratios in the melt during partial melting as a function of pressure and the percentage of garnet left in the residue. Partition coefficients at 23.5 GPa are from Walter et al. (2004). Data at 15 and 10 GPa are from this study. Partition coefficients for Gd and Yb were calculated using lattice strain model fits to partition coefficients for Sc, Lu, Y and Sm. Partition coefficients at 4.5 GPa are calculated using the data of Walter (1998) and the predictive model of van Westrenen et al. (2001). The grey area represents the compositional field of Archean Al-depleted komatiites from Barberton (Blichert-Toft and Arndt, 1999; Jahn et al., 1982; Jochum et al., 1991; Lahaye et al., 1995; Lecuyer et al., 1994; Parman et al., 2003; Sun and Nesbitt, 1978).



**Fig. 10.** Calculated rare earth element composition of hypothetical melts in equilibrium with natural majoritic garnets. See text for detailed calculation method. Depleted mantle composition from Salters and Stracke (2004); average MORB and OIB compositions from Sun and McDonough (1989); average kimberlite composition from Le Roex et al. (2003); average carbonatite composition from Bizimis et al. (2003). Compositions of majoritic garnet inclusions in diamonds are taken from Stachel et al. (2000) for Kankan diamonds, from Kaminsky et al. (2001) and Harte (1992) for Juina diamonds, from Tappert et al. (2005) for Jagersfontein diamonds, and from Moore et al. (1991) for Monastery diamonds.

enriched in both almandine and grossular components. A subduction-related origin for these diamonds provides a suitable explanation for the eclogitic major element compositions of their inclusions (e.g. Stachel et al., 2004; Tappert et al., 2005). The origin of the trace element signature has remained more uncertain. It could simply represent the trace signature of garnet in subducted slabs. It has also been proposed that the peculiar trace element signature of mineral inclusions such as majoritic garnet and calcium silicate perovskite reflects equilibration of these minerals with low-degree melts (Moore et al., 1991; Walter et al., 2008; Wang et al., 2000). Assuming majoritic garnets in diamonds are derived from or were in equilibrium with a melt at some stage prior to being trapped, one can calculate the rare earth element compositions of these hypothetical melts using the partitioning data from this study. Results of this calculation for representative majoritic garnet inclusions published in the literature are presented in Fig. 10. To account for the effect of pressure on partitioning, a correction was applied to $D_0$ using the following empirical relationship between $D_0^{3+}$ and pressure (P, in GPa) derived from data shown here:

$$D_0^{3+} = 1.669 + 0.1505\ P - 0.0101\ P^2. \tag{3}$$

As supported by our data ($E_X^{3+} = 665 \pm 41$ GPa, $r_0^{3+} = 0.922 \pm 0.001$ Å), we assume for the calculation that the variations in $E_X^{3+}$ and $r_0^{3+}$ with pressure are negligible at conditions of the transition zone. For each majoritic garnet inclusion, pressure was estimated from the Si content using the relationship displayed in Fig. 3 and temperature conditions are given by the mantle solidus (e.g. Herzberg et al., 2000). Partition coefficients for each REE at P–T conditions of interest were then calculated using Eq. (1). Given that the influence of temperature on the derived partition coefficients is rather small, the modelling remains valid when considering melting of various lithologies at lower temperature, provided that there is no strong compositional effect. No correction was made for the effect of composition on partitioning. As we discussed above, the addition of a large amount of $Fe^{2+}$ (almandine component) in the garnet structure is expected to

have a minor effect on garnet–melt partitioning. However, the addition of grossular component may have a larger influence. van Westrenen et al. (1999) have shown that at 3 GPa garnet–melt partition coefficients for light REE increase with increasing grossular content, in agreement with previous results by Harte and Kirkley (1997) for garnet–clinopyroxene partitioning. Although the variations in grossular content considered here are less extreme than in the study of van Westrenen et al. (1999), we caution that appropriate D values for light REE may be higher when considering majoritic garnet of eclogitic paragenesis. If the observations of van Westrenen et al. (1999) hold as well at higher pressures, calculated light REE contents in the hypothetical melts may be overestimated by up to an order of magnitude for La. As discussed below, such an overestimation would have no consequence on our interpretation. The results of Dalou et al. (2009), who studied trace element partitioning between majoritic garnet and carbonatitic melt at 20–25 GPa, indicate however that the effect of grossular content may be more limited than predicted by van Westrenen et al. (1999). Grossular rich-garnets (3 times the Ca content of that of peridotitic garnet) in the work of Dalou et al. (2009) are not particularly enriched in light REE. In fact, light REE display similar D values in both carbonatitic and peridotitic systems at similar pressures (Corgne and Wood, 2004; Dalou et al., 2009). In contrast, partition

coefficients for heavy REE are about 5 times higher in carbonatitic system than in peridotitic systems, with $D_{Lu}$ of about 5 and 1 respectively.

We calculated the REE composition of melts potentially in equilibrium with majoritic garnet inclusions from four localities: Monastery and Jagersfontein (South Africa), Kankan (Guinea), and Juina (Brazil). Results shown in Fig. 10 are compared with typical REE concentration patterns for mid-ocean ridge basalts (MORB), ocean island basalts (OIB), kimberlites, carbonatites, and the depleted mantle. The average MORB composition plots at the lower end of hypothetical parent melts. OIB, carbonatites and kimberlites have a REE signature that match best the calculated parent melt compositions. In detail, parent melts in equilibrium with Kankan inclusions would be very similar to kimberlites, whereas potential parent melts of the Juina inclusions would have a wide range of light REE concentrations, covering the compositional field of kimberlites, carbonatites and OIB. In comparison, potential parent melts for the Jagersfontein and Monastery diamonds would be slightly less enriched in light REE, with a compositional range varying between MORB and kimberlites. From the point of view of REE pattern, the above observations suggest that the melts hypothetically in equilibrium with majoritic garnet inclusions could represent a mixture of kimberlitic-, carbonatitic-, OIB- and MORB-like components, with Kankan possibly resembling a pure kimberlitic end-member. These conclusions are in agreement with the interpretation made by Wang et al. (2000) and Walter et al. (2008) that some silicate inclusions in diamonds may have crystallised from low-degree carbonatite melts in the deep mantle. Importantly, if one use majoritic garnet–carbonatite melt partition coefficients of Dalou et al. (2009) rather than partition coefficients of this study ($CO_2$-free system), the same overall interpretation can be made. In this case, hypothetical melts should be slightly more depleted in heavy REE.

It has been proposed that $CO_2$-rich melts such as kimberlites or carbonatites might have contributed to deep diamonds formation through carbonate reduction reactions ('redox freezing') that would occur when the melts migrate to areas such as the ambient mantle where oxygen fugacity is sufficiently low (e.g., Rohrbach and Schmidt, 2011). If this scenario occurs alongside majoritic garnet–melt equilibration, it could contribute to the negative Eu anomaly observed in the REE patterns of some majoritic garnet inclusions (e.g. Stachel et al., 2000; Tappert et al., 2005). Below the FMQ buffer, Eu is expected to be present as both $Eu^{2+}$ and $Eu^{3+}$, with predominance of the reduced form below IW-0.5 (Karner et al., 2010; Schreiber, 1987). Therefore at oxygen fugacity relevant to redox freezing (IW-1.5, Rohrbach and Schmidt, 2011), one should expect $Eu^{2+}$ to be largely predominant. From the lattice strain parabolas derived in this study (e.g. Fig. 5), partition coefficients for $Eu^{3+}$ and $Eu^{2+}$ would be ~0.12 and <0.04, respectively. Therefore, a larger proportion of $Eu^{2+}$ would decrease the bulk partition coefficient, and hence lower the Eu content in majoritic garnet. If $Eu^{2+}$ is predominant, one should therefore expect a bulk content at least 3 times lower than the one at conditions where $Eu^{3+}$ dominates (FMQ). This effect is thus sufficient to generate the range of negative Eu anomalies observed in majoritic garnet (Eu*/Eu down to 0.5, Tappert et al., 2005). Conversely, at relatively high oxygen fugacity, a positive Eu anomaly could be generated. High-pressure reduction reactions therefore provide a supplementary mechanism to generate Eu anomalies, in addition to the traditionally cited low-pressure fractionation/accumulation of plagioclase in oceanic crust protoliths (e.g. Stachel et al., 2004). If Eu anomalies result from crystallisation in redox gradients at high pressures, this also could mean that a negative Eu anomaly is not necessarily evidence that an inclusion had a basaltic protolith. It also means that positive Eu anomalies due to crystallisation from subducted crust could be 'erased' later on. Furthermore, the range of Eu anomalies observed in garnet inclusions in diamonds suggests that, if they are the result of transition zone or deep asthenospheric processes, the inclusions are forming in a range of different redox conditions. This is consistent with current models of deep diamond formation (e.g. Stachel et al., 2004; Tappert et al., 2005; Walter et al., 2008).

### 5.3. Crystallisation of the Martian magma ocean

Recent geochemical models of gross mantle differentiation in Mars invoke the crystallisation of a deep magma ocean (e.g. Borg and Draper, 2003; Debaille et al., 2009; Elkins-Tanton et al., 2005). Majoritic garnet plays a key role in these models because it would crystallise in fair amounts, on the order of 10 wt.%, (e.g. Borg and Draper, 2003; Elkins-Tanton et al., 2005), as it is thought to be the liquidus phase in Martian mantle compositions at pressures above 12 GPa and is a subliquidus phase at lowers pressures (e.g. Borg and Draper, 2003). More importantly, it is capable of fractionating key trace element pairs such as Sm/Nd and Lu/Hf (as shown in Fig. 5). Crystallisation of magma ocean cumulates in the presence of majoritic garnet would create a deep reservoir with relatively high Sm/Nd and Lu/Hf ratios, leading to large time-integrated $\varepsilon^{143}Nd$ and $\varepsilon^{176}Hf$. The concurrent crystallisation of olivine or one of its high-pressure polymorphs (wadsleyite and ringwoodite) would not affect significantly the Sm/Nd and Lu/Hf ratios, given the extremely low crystal–melt partition coefficients expected for these phases (Mibe et al., 2006).

Published models of Martian magma ocean differentiation use majoritic garnet/melt partition coefficients for Sm, Nd, Lu and Hf that were determined experimentally in the 5–7 GPa pressure range by Draper et al. (2003). However, a global Martian magma ocean could have reached depths of up to 2000 km deep, with a maximum pressure of 24 GPa (Bertka and Fei, 1997). The models of Borg and Draper (2003) and Elkins-Tanton et al. (2005) use maximum pressures of at least 15 GPa. We use the partition coefficients determined in the present study from 10 to 17 GPa as well as those from Corgne and Wood (2004) at 25 GPa to more accurately model garnet fractionation at the pressures expected for a deep Martian magma ocean.

Fig. 11 illustrates the variations of the Lu/Hf and Sm/Nd ratios of majoritic garnet-bearing cumulates normalised to initial source ratios as a function of the amount of crystallised majoritic garnet. As expected, the Lu/Hf and Sm/Nd signature of the majoritic reservoir is quite variable depending on pressure. Within the pressure range over which majorite would be expected to crystallise most (12–24 GPa), the majoritic reservoir would have a Sm/Nd ratio 2 to 4.5 times that of the magma ocean from which it crystallises. Modest (<10 GPa) and high (>20 GPa) pressure conditions would lead to $(Sm/Nd)_N$ of about 2–3. The highest fractionation would occur at intermediate pressures, with values of $(Sm/Nd)_N$ of about 4–4.5. Note that the derived Sm/Nd values are virtually independent from the size of the majoritic reservoir.

As for Lu/Hf, Fig. 11 indicates that fractionation at moderate (10 GPa) pressure and for an appropriate sized reservoir (~10% majoritic garnet ± ringwoodite) would lead to a cumulate Lu/Hf ratio of about 6 times that of the initial source. If fractionation occurs at higher pressure (>15 GPa), Lu/Hf is lower, about 4–5 times that of the initial source. Therefore, using partitioning data obtained at moderate pressures (5–7 GPa) to describe fractionation above 10 GPa as previously done by Borg and Draper (2003) and Elkins-Tanton et al. (2005) lead to a slight overestimation of the Lu/Hf ratio of the majoritic cumulates (curves ET05 and BD03 in Fig. 11). In turn, this would induce an underestimation of the Lu/Hf ratio of the residual magma ocean, appropriates values actually ranging between 0.9 and 0.95 of the initial Lu/Hf of the source.

### 6. Conclusions

Melting experiments were performed on a silica-rich peridotite composition at 10, 15 and 17 GPa to determine majoritic garnet–melt partition coefficients for a number of key elements. All elements investigated in this study are incompatible in majoritic garnet with the exceptions of Si, Al, Cr, Sc and Lu. As predicted from lattice strain considerations, log D for isovalent cations entering the large site of majoritic garnet exhibit a near-parabolic dependence on the ionic radius of incorporated cations. D values for many elements, including Na, Sc,
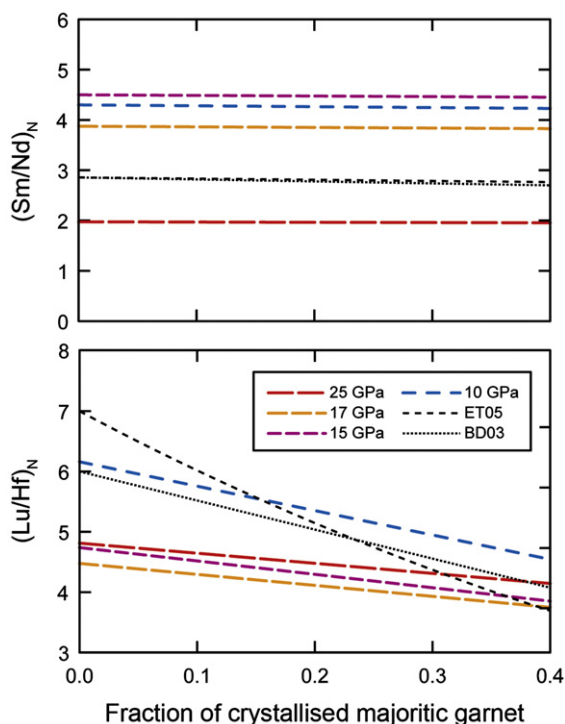
**Fig. 11.** (Lu/Hf) and (Sm/Nd) ratios of majoritic garnet cumulates normalised to source ratios calculated as a function of the fraction of crystallised majoritic garnet. Curves at 10, 15 and 17 GPa are derived from the partitioning data of this study. The 25 GPa curve is derived from the data of Corgne and Wood (2004). Curves labelled "ET05" and "BD03" are obtained from the partition coefficients used by Elkins-Tanton et al. (2005) and Borg and Draper (2003), respectively. Both these studies used partition coefficients from Draper et al. (2003) obtained in experiments at 5–7 GPa.

Y and REE, change significantly with increasing pressure or proportion of majorite component. $D_{Na}$ increases with increasing pressure, perhaps indicating that Na incorporation is charge-balanced by the coupled substitution of $Si^{4+}$–$Na^+$ for $Al^{3+}$–$M^{2+}$. Lu and Sc become incompatible at 17 GPa, with partition coefficients decreasing from about 1.5 at 10 GPa to 0.9 at 17 GPa. The negative correlation between $D_{Si}$ and $D_o^{3+}$ indicates that the charge-balancing mechanisms for the incorporation of Si in the Y-site and large trivalent cations in the X-site are competing.

With the new data obtained here, we refined the predictive model of van Westrenen and Draper (2007) for garnet–melt partitioning of trivalent cations, which was initially constructed from a data set lacking inputs in the 10–20 GPa range. Eq. (2) of this contribution together with Eqs. (3) and (6) of van Westrenen and Draper (2007) now provides a more robust prediction of REE garnet–melt partitioning over the entire garnet stability field, with a resolution matching that of the empirical predictive model of Draper and van Westrenen (2007).

Using our new data, we suggest that Archean Al-depleted komatiites from Barberton may have been generated by partial melting of anhydrous peridotite in the presence of residual garnet at depths between 200 and 400 km, but not at greater depths as previously suggested. The addition of water would not have a significant effect in terms of the pressure range and proportion of garnet removal required. Our data also indicate that transition zone diamonds from Kankan may have formed from reduction of deep $CO_2$-rich magmas that subsequently transported them to the surface. This possibility would provide an explanation for the REE patterns of majoritic garnet trapped within these diamonds, including the presence of Eu anomalies. Finally, our data are used to illustrate that segregation of majoritic garnet-bearing cumulates from a deep Martian magma ocean could lead to a variety of Lu/Hf and Sm/Nd ratios depending on the depth of crystallisation, creating a range of possible $\varepsilon^{143}Nd$ and $\varepsilon^{176}Hf$ isotope signatures for Martian mantle sources.

## References

Akaogi, M., Akimoto, S., 1979. High-pressure phase equilibria in a garnet lherzolite, with special reference to $Mg^{2+}$–$Fe^{2+}$ partitioning among constituent minerals. Physics of the Earth and Planetary Interiors 19, 31–51.

Arndt, N.T., 1986. Komatiites: a dirty window to the Archean mantle. Terra Cognita 6, 9–66.

Bertka, C.M., Fei, Y., 1997. Mineralogy of the Martian interior up to core–mantle boundary pressures. Journal of Geophysical Research 102, 5251–5264.

Bizimis, M., Salters, V.J.M., Dawson, J.B., 2003. The brevity of carbonatite sources in the mantle: evidence from Hf isotopes. Contributions to Mineralogy and Petrology 145, 281–300.

Blichert-Toft, J., Arndt, N.T., 1999. Hf isotope geochemistry of komatiites. Earth and Planetary Science Letters 171, 439–451.

Blundy, J.D., Wood, B.J., 1994. Prediction of crystal–melt partitioning coefficients from lattice elastic moduli. Nature 372, 452–454.

Borg, L.E., Draper, D.S., 2003. A petrogenetic model for the origin and compositional variation of the martian basaltic meteorites. Meteoritics and Planetary Science 38, 1713–1731.

Brice, J.C., 1975. Some thermodynamic aspects of the growth of strained crystals. Journal of Crystal Growth 28, 246–253.

Collerson, K.D., Hapugoda, S., Kamber, B.S., Williams, Q., 2000. Rocks from the mantle transition zone: majorite-bearing xenoliths from Malaita, Southwest Pacific. Science 288, 1215–1223.

Collerson, K.D., Williams, Q., Kamber, B.S., Omori, S., Arai, H., Ohtani, E., 2010. Majoritic garnet: a new approach to pressure estimation of shock events in meteorites and the encapsulation of sub-lithospheric inclusions in diamond. Geochimica et Cosmochimica Acta 74, 5939–5957.

Corgne, A., Wood, B.J., 2002. $CaSiO_3$ and $CaTiO_3$ perovskite–melt partitioning of trace elements: implications for gross mantle differentiation. Geophysical Research Letters 29, 1933, http://dx.doi.org/10.1029/2001GL014398.

Corgne, A., Wood, B.J., 2004. Trace element partitioning between majoritic garnet and silicate melt at 25 GPa. Physics of the Earth and Planetary Interiors 143, 407–419.

Corgne, A., Wood, B.J., 2005. Trace element partitioning and substitution mechanisms in calcium silicate perovskites. Contributions to Mineralogy and Petrology 149, 85–97.

Corgne, A., Allan, N.L., Wood, B.J., 2003. Atomistic simulations of trace element incorporation into the large site of $MgSiO_3$ and $CaSiO_3$ perovskites. Physics of the Earth and Planetary Interiors 139, 113–127.

Dalou, C., Koga, K.T., Hammouda, T., Poitrasson, F., 2009. Trace element partitioning between carbonatitic melts and mantle transition zone minerals: implications for the source of carbonatites. Geochimica et Cosmochimica Acta 73, 239–255.

Debaille, V., Brandon, A.D., O'Neill, C., Yin, Q.-Z., Jacobsen, B., 2009. Early martian mantle overturn inferred from isotopic composition of nakhlite meteorites. Nature Geoscience 2, 548–552.

Draper, D.S., van Westrenen, W., 2007. Quantifying garnet–melt trace element partitioning using lattice-strain theory: assessment of statistically significant controls and a new predictive model. Contributions to Mineralogy and Petrology 154, 731–746.

Draper, D.S., Xirouchakis, D., Agee, C.B., 2003. Trace element partitioning between garnet and chondritic melt from 5 to 9 GPa: implications for the onset of the majorite transition in the martian mantle. Physics of the Earth and Planetary Interiors 139, 149–169.

Dwarzski, R.E., Draper, D.S., Shearer, C.K., Agee, C.B., 2006. Experimental insights on crystal chemistry of high-Ti garnets from garnet–melt partitioning of rare-earth and high-field-strength elements. American Mineralogist 91, 1536–1546.

Elkins-Tanton, L.T., Hess, P.C., Parmentier, E.M., 2005. Possible formation of ancient crust on Mars through magma ocean processes. Journal of Geophysical Research 110, E12S01, http://dx.doi.org/10.1029/2005JE002480.

Fujinawa, A., Green, T.H., 1997. Partitioning behaviour of Hf and Zr between amphibole, clinopyroxene, garnet and silicate melts at high pressure. European Journal of Mineralogy 9, 379–391.

Gasparik, T., 1990. Phase relations in the transition zone. Journal of Geophysical Research 95, 15751–15769.

Green, D.H., 1975. Genesis of Archean peridotitic magmas and constraints on Archean geothermal gradients and tectonics. Geology 3, 15–18.

Grove, T.L., Gaetani, G.A., deWit, M.J., 1994. Spinifex textures in 3.49 Ga Barberton Mountain belt komatiites: evidence for crystallization of water-bearing, cool magmas in the Archean. EOS Transactions of the American Geophysical Union 75, 354.

Gudfinnsson, G.H., Presnall, D.C., 1996. Melting relations of model lherzolite in the system CaO-MgO-Al$_2$O$_3$-SiO$_2$ at 2.4–3.4 GPa and the generation of komatiites. Journal of Geophysical Research 101, 27701–27709.

Harte, B., 1992. Trace element characteristics of deep-seated eclogite parageneses—an ion microprobe study of inclusions in diamonds. VM Goldschmidt Conference: The Geochemical Society, Reston, VA, p. A48.

Harte, B., Kirkley, M.B., 1997. Partitioning of trace elements between clinopyroxene and garnet: data from mantle eclogites. Chemical Geology 136, 1–24.

Hauri, E.H., Wagner, T.P., Grove, T.L., 1994. Experimental and natural partitioning of Th, U, Pb and other trace elements between garnet, clinopyroxene and basaltic melts. Chemical Geology 117, 149–166.

Heinemann, S., Sharp, T.G., Seifert, F., Rubie, D.C., 1997. The cubic–tetragonal phase transition in the system majorite (Mg$_4$Si$_4$O12), pyrope (Mg$_3$Al2Si3O12), and garnet symmetry in the earth's transition zone. Physics and Chemistry of Minerals 24, 206–221.

Herzberg, C., 1992. Depth and degree of melting of komatiites. Journal of Geophysical Research 97, 4521–4540.

Herzberg, C., 1995. Generation of plume magmas through time: an experimental perspective. Chemical Geology 126, 1–16.

Herzberg, C., Zhang, J., 1996. Melting experiments on anhydrous peridotite KLB-1: compositions of magmas in the upper mantle and transition zone. Journal of Geophysical Research 101, 8271–8295.

Herzberg, C., Raterron, P., Zhang, J., 2000. New experimental observations on the anhydrous solidus for peridotite KLB-1. Geochemistry, Geophysics, Geosystems 1, http://dx.doi.org/10.1029/2000GC000089.

Hirose, K., 2002. Phase transitions in pyrolitic mantle around 670-km depth: implications for upwelling of plumes from the lower mantle. Journal of Geophysical Research 107, http://dx.doi.org/10.1029/2001JB000597.

Inoue, T., Rapp, R.P., Zhang, J., Gasparik, T., Weidner, D.J., Irifune, T., 2000. Garnet fractionation in a hydrous magma ocean and the origin of Al-depleted komatiites: melting experiments of hydrous pyrolite with REEs at high pressure. Earth and Planetary Science Letters 177, 81–87.

Irifune, T., 1987. An experimental investigation of the pyroxene–garnet transition in a pyrolite composition and its bearing on the constitution of the mantle. Earth and Planetary Science Letters 45, 324–336.

Irifune, T., Hibberson, W.O., Ringwood, A.E., 1989. Eclogite–garnetite transformation at high pressure and its bearing on the occurrence of garnet inclusions in diamond. In: Ross, J., et al. (Ed.), Kimberlites and Related Rocks. : Special Publications no. 14 of the Geological Society of Australia. Blackwell, Carlton, pp. 877–882.

Ito, E., Takahashi, E., 1987. Melting of peridotite at uppermost lower-mantle conditions. Nature 328, 514–517.

Jahn, B.M., Gruau, G., Glikson, A.Y., 1982. Komatiite of Onverwacht Group, South Africa: REE geochemistry, Sm/Nd age and mantle evolution. Contributions to Mineralogy and Petrology 80, 25–40.

Jochum, K.P., Arndt, N.T., Hofmann, A.W., 1991. Nb–Th–La in komatiites and basalts: constraints on komatiite petrogenesis and mantle evolution. Earth and Planetary Science Letters 107, 272–289.

Johnson, K.T.M., 1998. Experimental determination of partition coefficients for rare earth and high-field-strength elements between clinopyroxene, garnet, and basaltic melt at high pressures. Contributions to Mineralogy and Petrology 133, 60–68.

Kaminsky, F.V., Zakharchenko, O.D., Davies, R.M., Griffin, W.L., Khachatryan-Blinova, G.K., Shiryaev, A.A., 2001. Superdeep diamonds from the Juina aera, Mato Grosso State, Brazil. Contributions to Mineralogy and Petrology 140, 734–753.

Karner, J.M., Papike, J.J., Sutton, S.R., Burger, P.V., Shearer, C.K., Le, L., Newville, M., Choi, Y., 2010. Partitioning of Eu between augite and a highly spiked martian basalt composition as a function of oxygen fugacity (IW-1 to QFM): determination of Eu$^{2+}$/Eu$^{3+}$ ratios by XANES. American Mineralogist 95, 410–413.

Kato, T., Ringwood, A.E., Irifune, T., 1988. Experimental determination of element partitioning between silicate perovksites, garnets and liquids: constraints on early differentiation of the mantle. Earth and Planetary Science Letters 89, 123–145.

Katsura, T., Yamada, H., Nishikawa, O., Song, M., Kubo, A., Shinmei, T., Yokoshi, S., Aizawa, Y., Yoshino, T., Walter, M.J., Ito, E., 2004. Olivine–wadsleyite transition in the system (Mg, Fe)2SiO4. Journal of Geophysical Research 109, http://dx.doi.org/10.1029/2003JB002438.

Keshav, S., Sen, G., 2001. Majoritic garnets in the Hawaiian xenoliths: preliminary results. Geophysical Research Letters 28, 3509–3512.

Lahaye, Y., Arndt, N., Byerly, G., Chauvel, C., Fourcade, S., Gruau, G., 1995. The influence of alteration on the trace-element and Nd isotopic compositions of komatiites. Chemical Geology 126, 43–64.

Le Roex, A.P., Bell, D.R., Davis, P., 2003. Petrogenesis of Group I Kimberlites from Kimberley, South Africa: evidence from bulk-rock geochemistry. Journal of Petrology 44, 2261–2286.

Lecuyer, C., Gruau, G., Anhaeusser, C.R., Fourcade, S., 1994. The origin of fluids and the effects of metamorphism on the primary chemical compositions of Barberton komatiites: new evidence from geochemical (REE) and isotopic (Nd, O, H, $^{39}$Ar/$^{40}$Ar) data. Geochimica et Cosmochimica Acta 58, 969–984.

Lesher, C.E., Pickering-Witter, J., Baxter, G., Walter, M., 2003. Melting of garnet peridotite: effects of capsules and thermocouples, and implications for the high-pressure mantle solidus. American Mineralogist 88, 1181–1189.

Litasov, K., Ohtani, E., 2003. Hydrous solidus of CMAS-pyrolite and melting of mantle plumes at the bottom of the upper mantle. Geophysical Research Letters 30, 2143, http://dx.doi.org/10.1029/2003GL018318.

McCammon, C.A., Ross, N.L., 2003. Crystal chemistry of ferric iron in (Mg, Fe)(Si, Al)O3 majorite with implications for the transition zone. Physics and Chemistry of Minerals 30, 206–216.

McDonough, W.F., Sun, S.S., 1995. The composition of the Earth. Chemical Geology 120, 223–253.

Mibe, K., Orihashi, Y., Nakai, S., Fujii, T., 2006. Element partitioning between transition-zone minerals and ultramafic melt under hydrous conditions. Geophysical Research Letters 33, http://dx.doi.org/10.1029/2006GL026999.

Moore, R.O., Gurney, J.J., 1985. Pyroxene solid solution in garnets included in diamonds. Nature 318, 553–555.

Moore, R.O., Gurney, J.J., Griffin, W.L., Shimizu, N., 1991. Ultra-high pressure garnet inclusions in Monastery diamonds: trace element abundance patterns and conditions of origin. European Journal of Mineralogy 3, 213–230.

Nicholls, I.A., Harris, K.L., 1980. Experimental rare earth element partition coefficients for garnet, clinopyroxene and amphibole coexisting with andesitic and basaltic liquids. Geochimica et Cosmochimica Acta 44, 287–308.

Niyashima, N., Yagi, T., 2004. Phase relation and mineral chemistry in pyrolite to 2200 °C under the lower mantle pressures and implications for dynamics of mantle plumes. Journal of Geophysical Research 108, http://dx.doi.org/10.1029/2002JB002216.

Ohtani, E., Kato, T., Sawamoto, H., 1986. Melting of a model chondritic mantle to 20 GPa. Nature 322, 352–353.

Ohtani, E., Kawabe, I., Moriyama, J., Nagata, Y., 1989. Partitioning of elements between majorite garnet and melt and implications for the petrogenesis of komatiite. Contributions to Mineralogy and Petrology 103, 263–269.

Ono, S., Yasuda, A., 1996. Compositional change of majoritic garnet in a MORB composition from 7 to 17 GPa and 1400 to 1600 °C. Physics of the Earth and Planetary Interiors 96, 171–176.

Onuma, N., Higuchi, H., Wakita, H., Nagasawa, H., 1968. Trace element partition between two pyroxenes and the host lava. Earth and Planetary Science Letters 5, 47–51.

Parman, S.W., Dann, J.C., Grove, T.L., deWit, M.J., 1997. Emplacement conditions of komatiite magmas from the 3.49 Ga Komati Formation, Barberton Greenstone Belt, South Africa. Earth and Planetary Science Letters 150, 303–323.

Parman, S.W., Shimizu, N., Grove, T.L., Dann, J.C., 2003. Constraints on the pre-metamorphic trace element composition of Barberton komatiites from ion probe analyses of preserved clinopyroxene. Contributions to Mineralogy and Petrology 144, 383–396.

Quartieri, S., Antonioli, G., Geiger, C.A., Artioli, G., Lottici, P.P., 1999. XAFS characterization of the structural site of Yb in synthetic pyrope and grossular garnets. Physics and Chemsitry of Minerals 26, 251–256.

Ringwood, A.E., 1991. Phase transformations and their bearing on the constitution and dynamics of the mantle. Geochimica et Cosmochimica Acta 55, 2083–2110.

Rohrbach, A., Schmidt, M.W., 2011. Redox freezing and melting in the Earth's deep mantle resulting from carbon–iron redox coupling. Nature 472, 209–212.

Salters, V.J.M., Longhi, J., 1999. Trace element partitioning during the initial stages of melting beneath mid-ocean ridges. Earth and Planetary Science Letters 166, 15–30.

Salters, V.J.M., Stracke, A., 2004. Composition of the depleted mantle. Geochemistry, Geophysics, Geosystems 5, http://dx.doi.org/10.1029/2003GC000597.

Schreiber, H.D., 1987. An electrochemical series of redox couples in silicate melts: a review and applications to geochemistry. Journal of Geophysical Research 92, 9225–9232.

Shimizu, N., Kushiro, I., 1975. The partitioning of rare earth elements between garnet and liquid at high pressures: preliminary experiments. Geophysical Research Letters 2, 413–416.

Smyth, J.R., Bish, D.L., 1988. Crystal Structures and Cation Sites of the Rock-forming Minerals. Allen and Unwin, London.

Stachel, T., Brey, G.P., Harris, J.W., 2000. Kankan diamonds (Guinea) I: from the lithosphere down to the transition zone. Contributions to Mineralogy and Petrology 140, 1–15.

Stachel, T., Aulbach, S., Brey, G.P., Harris, J.W., Leost, I., Tappert, R., Viljoen, K.S., 2004. The trace element composition of silicate inclusions in diamonds: a review. Lithos 77, 1–19.

Sun, S.S., McDonough, W.F., 1989. Chemical and isotopic systematics of oceanic basalts: implications for mantle composition and processes. In: Saunders, A.D., Norry, M.J. (Eds.), Magmatism in the Ocean Basins, vol 42. Geochemical Society Special Publications, London, pp. 313–345.

Sun, S.S., Nesbitt, R.W., 1978. Petrogenesis of Archean ultrabasic and basic volcanics: evidence from rare earth elements. Contributions to Mineralogy and Petrology 65, 301–325.

Suzuki, T., Akaogi, M., Nakamura, E., 2000. Partitioning of major elements between garnet-structured minerals and silicate melt at pressure of 3–15 GPa. Physics of the Earth and Planetary Interiors 120, 79–92.

Takahashi, E., 1990. Speculations on the Archean mantle: missing link between komatiite and depleted garnet peridotite. Journal of Geophysical Research 95, 15941–15954.

Takahashi, E., Scarfe, C.M., 1985. Melting of peridotite to 14 GPa and the genesis of komatiite. Nature 315, 566–568.

Tappert, R., Stachel, T., Harris, J.W., Muehlenbachs, K., Ludwig, T., Brey, G.P., 2005. Subducting oceanic crust: the source of deep diamonds. Geology 33, 565–568.

Trønnes, R.G., Frost, D.J., 2002. Peridotite melting and mineral–melt partitioning of major and minor elements at 21–24 GPa. Earth and Planetary Science Letters 197, 117–131.

Trønnes, R.G., Canil, D., Wei, K., 1992. Element partitioning between silicate minerals and coexisting melts at pressures of 1–27 GPa, and implications for mantle evolution. Earth and Planetary Science Letters 111, 241–255.

van Westrenen, W., Draper, D.S., 2007. Quantifying garnet–melt trace element partitioning using lattice-strain theory: new crystal-chemical and thermodynamic constraints. Contributions to Mineralogy and Petrology 154, 717–730.

van Westrenen, W., Blundy, J.D., Wood, B.J., 1999. Crystal-chemical controls on trace element partitioning between garnet and anhydrous silicate melt. American Mineralogist 84, 838–847.

van Westrenen, W., Blundy, J.D., Wood, B.J., 2000a. Effect of $Fe^{2+}$ on garnet–melt trace element partitioning: experiments in FCMAS and quantification of crystal-chemical controls in natural systems. Lithos 53, 191–203.

van Westrenen, W., Allan, N.L., Blundy, J.D., Purton, J.A., Wood, B.J., 2000b. Atomistic simulation of trace element incorporation into garnets—comparison with experimental garnet–melt partitioning data. Geochimica et Cosmochimica Acta 64, 1629–1639.

van Westrenen, W., Blundy, J.D., Wood, B.J., 2001. A predictive thermodynamic model of garnet–melt trace element partitioning. Contributions to Mineralogy and Petrology 142, 219–234.

van Westrenen, W., Van Orman, J.A., Watson, H., Fei, Y., Watson, E.B., 2003. Assessment of temperature gradients in multianvil assemblies using spinel layer growth kinetics. Geochemistry Geophysics Geosystems 4, 1036.

Walter, M.J., 1998. Melting of garnet peridotite and the origin of komatiite and depleted lithosphere. Journal of Petrology 39, 29–60.

Walter, M.J., Thibault, Y., Wei, K., Luth, R.W., 1995. Characterizating experimental pressure and temperature conditions in multi-anvil apparatus. Canadian Journal of Physics 73, 273–286.

Walter, M.J., Nakamura, E., Trønnes, R.G., Frost, D.J., 2004. Experimental constraints on crystallization differentiation in a deep magma ocean. Geochimica et Cosmochimica Acta 68, 4267–4284.

Walter, M.J., Bulanova, G.P., Armstrong, L.S., Keshav, S., Blundy, J.D., Gudfinnsson, G., Lord, O.T., Lennie, A.R., Clark, S.M., Smith, C.B., Gobbo, L., 2008. Primary carbonatite melt from deeply subducted oceanic crust. Nature 454, 622–625.

Wang, W., Takahashi, E., 2000. Subsolidus and melting experiments of K-doped peridotite KLB-1 to 27 GPa: its geophysical and geochemical implications. Journal of Geophysical Research 105, 2855–2868.

Wang, W., Gasparik, T., Rapp, R.P., 2000. Partitioning of rare earth elements between $CaSiO_3$ perovskite and coexisting phases: constraints on the formation of $CaSiO_3$ inclusions in diamonds. Earth and Planetary Science Letters 181, 291–300.

Wood, B.J., 2000. Phase transformations and partitioning relations in peridotite under lower mantle conditions. Earth and Planetary Science Letters 174, 341–354.

Wood, B.J., Blundy, J.D., 2001. The effect of cation charge on crystal–melt partitioning of trace elements. Earth and Planetary Science Letters 188, 59–71.

Wood, B.J., Blundy, J.D., 2002. The effect of $H_2O$ on crystal–melt partitioning of trace elements. Geochimica et Cosmochimica Acta 66, 3647–3656.

Yurimoto, J., Ohtani, E., 1992. Element partitioning between majorite and liquid: a secondary ion mass spectrometric study. Geophysical Research Letters 19, 17–20.

Zhang, J., Herzberg, C., 1994. Melting experiments on anhydrous peridotite KLB-1 from 5.0 to 22.5 GPa. Journal of Geophysical Research 99, 17729–17742.

Zhang, J., Li, B., Utsumi, W., Liebermann, R.C., 1996. In situ X-ray observations of the coesite–stishovite transition: reversed phase boundary and kinetics. Physics and Chemistry of Minerals 23, 1–10.